Spectra–Structure Correlations in Raman Spectroscopy

H.G.M. Edwards
University of Bradford, Bradford, UK

1 FACTORS THAT AFFECT RAMAN BAND PARAMETERS

The four parameters that are normally available from Raman spectral analysis and that are useful for the assignment of vibrational modes and characterization of the molecular structures of chemical species may be summarized as follows:

$\tilde{\nu}$ (cm^{-1})	The wavenumber position
$\Delta\tilde{\nu}_{1/2}$ (cm^{-1})	The bandwidths, usually expressed as FWHM (full width at half-maximum) or as HWHM (half width at half-maximum)
I (W sr^{-1})	The band intensity, which is often expressed in a relatively subjective way, such as strong, medium or weak
ρ	The depolarization ratio, which may provide good supporting evidence for molecular vibrational assignments

The interplay of these factors with each other and between neighboring molecules is often complex and the values of the wavenumber, bandwidth, band intensity and depolarization ratio will change with temperature of the system, molecular orientations in condensed phases, and the molecular environments. Additionally, the geometric– optical effects of various sample illumination geometries and mountings in use currently, convolved with different laser excitation wavelengths and spectral data accumulation conditions, such as spectral resolution and signal-to-noise ratios, can all conspire to alter the appearance of Raman spectra obtained from one laboratory to another.

This results in considerable expertise often being necessary for the interpretation of Raman spectra of complex molecular systems and the difficulties of keying in procedures to Raman databases. Basically, the following criteria apply for the structural interpretation of Raman spectra, which can now be excited using laser wavelengths operating from the deep ultraviolet (UV) near 240 nm, through the visible region (with commonly used excitation wavelengths at 488, 515, 530 and 633 nm) into the far red and near-infrared, where common excitation wavelengths of 780, 852 and 1064 nm are adopted. Recently, there has been a report of the first successful Raman spectra recorded using 1330 nm excitation.[1] Being a light-scattering effect, Raman spectroscopy using such a diverse range of wavelengths from the UV to the infrared (IR), can also create problems for the analytical spectroscopist working with sensitive and colored materials, because of the onset of specimen degradation, fluorescence emission and resonance scattering effects.[2]

The excitation of Raman spectra in the UV and visible blue/green spectral regions can cause problems with fluorescence generation, which may be several orders of magnitude larger than the relatively weak Raman spectral bands, and, worse, may result in a spectral degeneration caused by sample absorption and decomposition. This is especially true if laser Raman microscopy is used as an analytical technique at shorter wavelengths, where great care must be taken to maintain the irradiance (W m^{-2}) at the sample at a small level. For example, in a conventional Raman spectrometer, where the sample spot size may be 100 μm in diameter, the reduction in sampling dimension offered by Raman microscopy will provide an increase in

---

Handbook of Vibrational Spectroscopy, Online © 2006 John Wiley & Sons, Ltd.

This article was published in the *Handbook of Vibrational Spectroscopy* in 2006 by John Wiley & Sons, Ltd.
DOI: 10.1002/9780470027325.s4103

the irradiance at the specimen of a factor of up to $10^3\times$ or more, depending on the magnification of the microscope objective used. Hence, a 10 mW laser power incident on the sample for macroscopic imaging results in a power density of 1000× more for the same laser power in the microscopic mode. For insensitive materials, the scattered Raman radiation is correspondingly greater, but biological materials often suffer at these high power densities – and the spectral appearance is changed.

The advantage of working at lower wavelength, λ, excitation is clear from the intensity of Raman scattering, which is dependent on λ^{-4}. Hence, the Raman spectrum of a sample recorded at 1065 nm is about 250× weaker intrinsically than that recorded at 240 nm; the advantage of moving to long wavelength excitation is the preservation of sample integrity with use of lower energy sources and the suppression of fluorescence, resulting in improved spectral quality.[3]

Colored materials, which may have electronic absorption bands in the visible near the wavelength of laser excitation, can cause problems of a different nature for spectral interpretation as the onset of preresonance or strict resonance Raman scattering (RRS) can occur. The RRS is used to enhance the weak Raman scattering observed from low-concentration species by up to $10^5\times$, but only selected vibrational features are enhanced in this way – specifically, those that have a vibrational association with the electronic transition that is closest to the resonant laser wavelength. The appearance of the Raman spectrum in RRS is, therefore, very different from that observed in normal Raman scattering, with certain vibrational bands appearing very intense and others by comparison being only weakly present or not observed at all. An example is shown in Figure 1, with the excitation of Raman spectra from a colored inorganic pigment using different visible laser wavelengths, one of which is absorbed by the specimen, causing heating and sample degradation.

Likewise, the wavenumbers and bandwidths of Raman bands will invariably change to a greater or lesser extent depending on the state of matter that applies to the spectra and, more importantly, on the presence of molecules in the system, which may provide a different electronic or chemical environment for the species under study. This has been a very rich area for analytical Raman spectroscopy and several examples will be used to illustrate applications later in this article, taken from the areas of ionic solvation in mixed solvent systems, hydrogen-bonded systems and the spectroscopic study of equilibria such as stepwise complex formation or keto–enol tautomerization. In these studies, not only do the wavenumbers change, for example, reflecting the difference in the vibrational modes of M^{n+}(aq), M^{n+}(solv), $M^{n+}X^{m-}$ ion pairing and $(M–X)^{(n-m)+}$ co-ordination in ionic salt dissociation in a mixed aqueous–organic solvent system, but spectral bandwidths change according to the spectroscopic resolution that applies. Hence, the asymmetry of a complex vibrational Raman feature recorded with specific spectral resolution may be of a different appearance under higher resolution, when several spectral features have now been resolved. The application of spectral deconvolution techniques to identify band components in poorly resolved Raman features is well illustrated for a complex biological feature, namely human skin (Figure 2); this provides an important topic for the biomedical diagnostic applications of modern Raman spectroscopic techniques.[4]

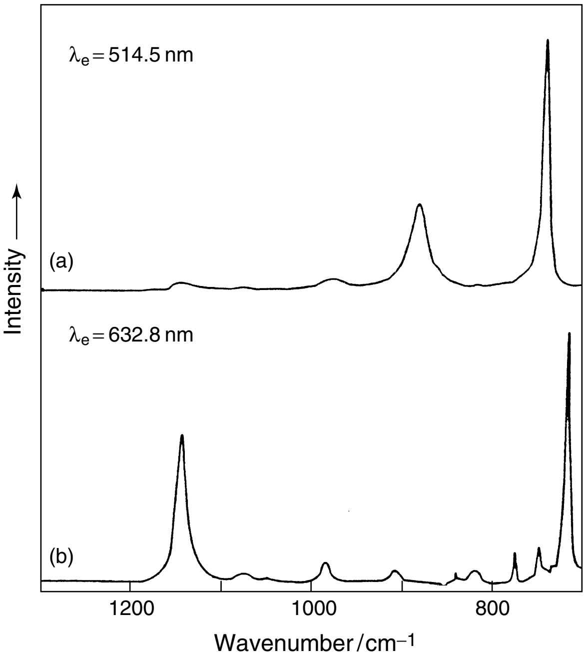

Figure 1. Effect of excitation wavelength on Raman band intensities – the Raman spectrum of lead(II) lead(IV) tetroxide (red lead), Pb_3O_4, excited with (a) 514.5 nm and (b) 632.8 nm laser radiation. The genuine spectrum of this important pigment is (b); the spectrum excited by the green radiation in (a) corresponds to massicot, PbO, which is a decomposition product of Pb_3O_4 initiated by laser absorption and localized heating of the specimen. [Reproduced with permission of Pergamon Press Ltd., S.J. Best, R.J.H. Clark and R. Withnall, *Endeavour*, **16**(2), 66 (1992).]

Single crystals, particularly microcrystals, being studied by Raman microscopy will exhibit a different Raman spectral appearance under different orientations in sample illumination because of polarization effects, which depend on the combination of the incident electric vector and the scattering geometry of the molecular crystal system. Effectively, this too can create spectral differences that can trap the unwary. However, for many analytical applications requiring finely ground solid material, this problem is not experienced in Raman spectroscopy.

Finally, a major difference in the observation of Raman and IR spectra lies in the spectral ranges covered by Raman spectrometers, which typically cover 50–3500 cm^{-1} in one

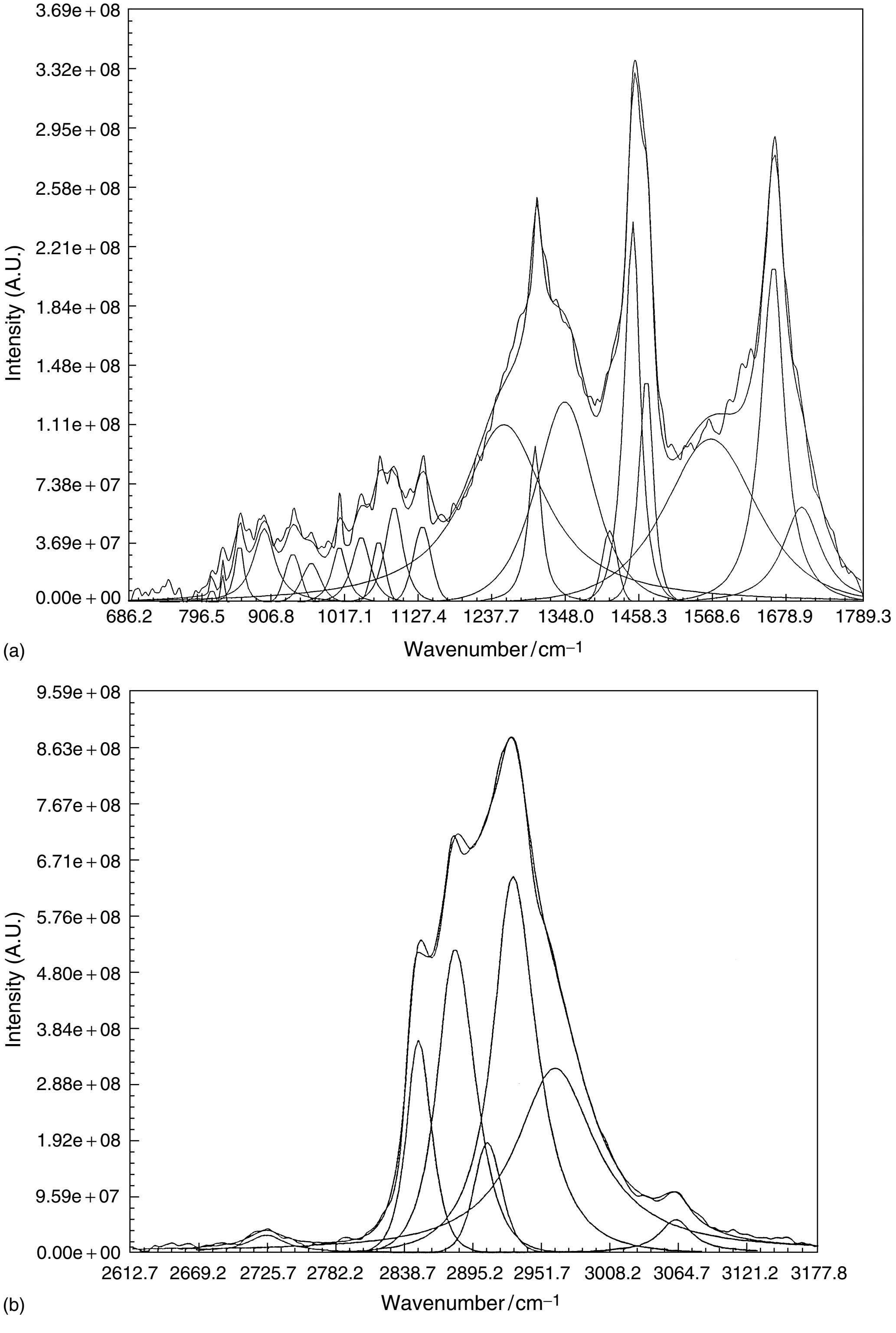

Figure 2. Fourier transform (FT) self-deconvolution of the Raman spectra of a complex biomaterial – 1064 nm excitation, 4000 scans, $4\,\mathrm{cm}^{-1}$ spectral resolution of (a) and (b) contemporary human skin and (c) and (d) skin of the Alpine Iceman, 5200 y BP for the spectral wavenumber regions $\Delta\nu = 2610–3170$ and $690–1790\,\mathrm{cm}^{-1}$. The upper spectra are recorded experimentally, and the lower spectra are deconvoluted bands, illustrating the complex envelope of a biopolymer in the ν(CH) and functionality regions. The effect of environmental degradation on the archaeological biotissue can be clearly seen by comparison. [Reproduced with permission of the Royal Society of Chemistry from H.G.M. Edwards, A.C. Williams, D.W. Farwell, B.W. Barry and F. Rull, *J. Chem. Soc., Faraday Trans.*, **91**, 3883–3887 (1995).]

Handbook of Vibrational Spectroscopy, Online © 2006 John Wiley & Sons, Ltd.

This article was published in the *Handbook of Vibrational Spectroscopy* in 2006 by John Wiley & Sons, Ltd.
DOI: 10.1002/9780470027325.s4103

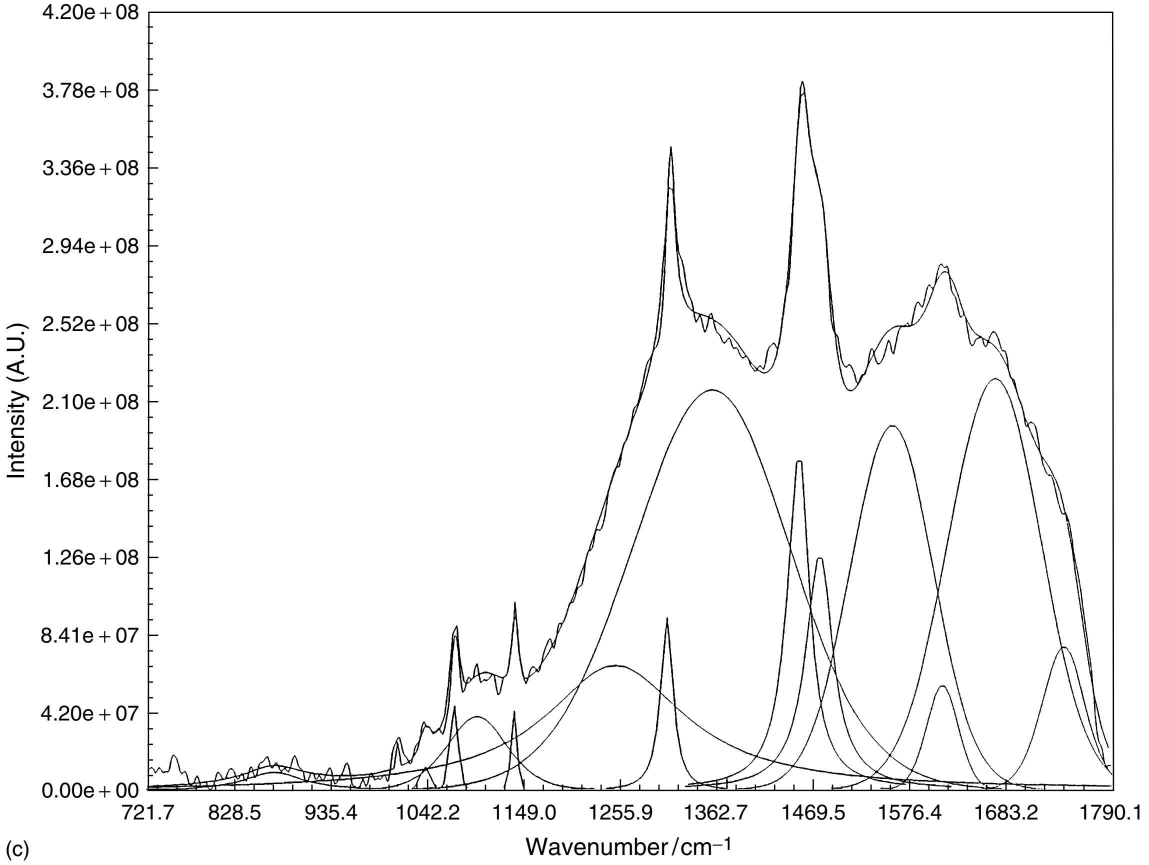

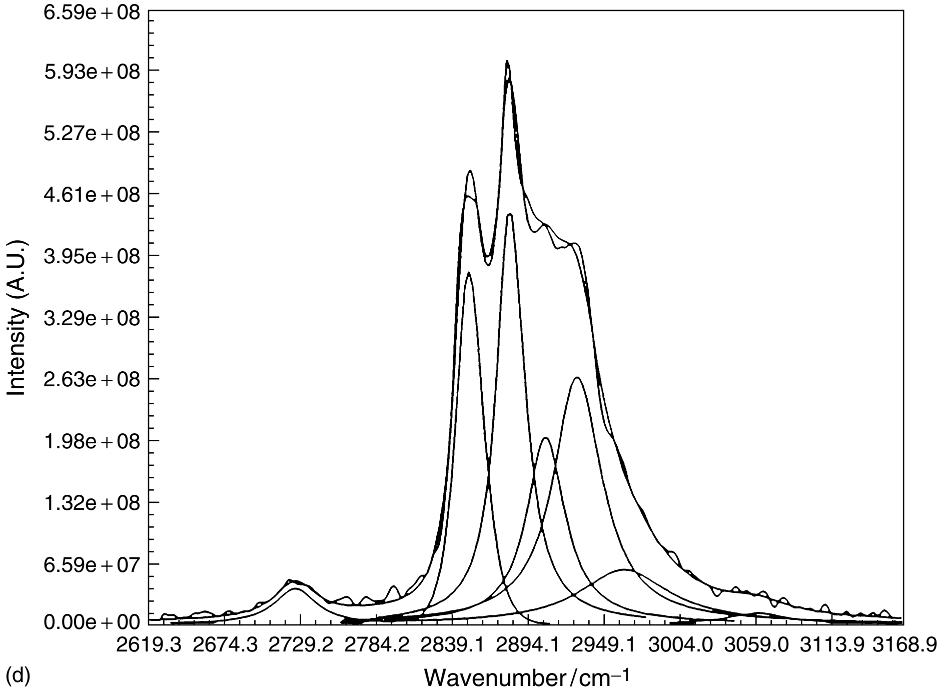

Figure 2. (*Continued*)

DOI: 10.1002/9780470027325.s4103

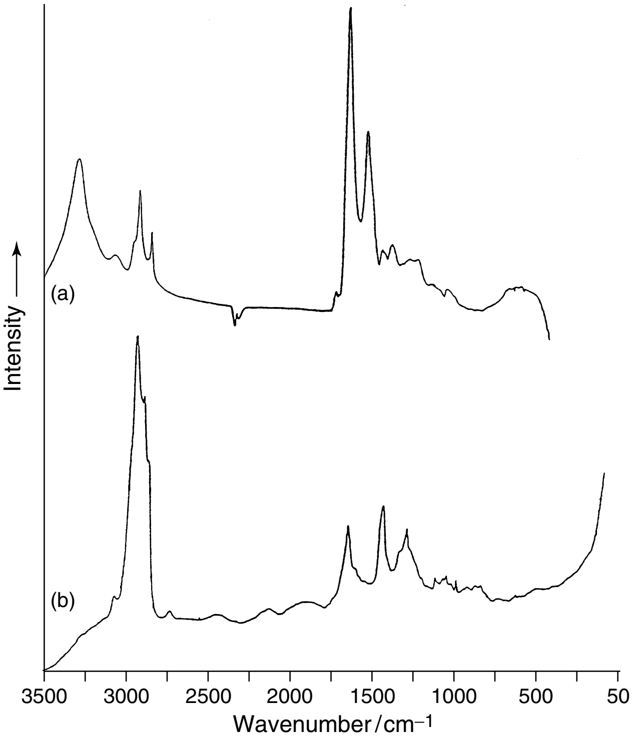

Figure 3. Comparison of IR and Raman spectra of human skin tissue in the wavenumber range 50–3500 cm^{-1} maximum. (a) FT-IR of desiccated specimen; (b) FT-Raman spectrum (1064 nm excitation) of naturally hydrated specimen. [Reproduced with permission of Elsevier Science from A.C. Williams, H.G.M. Edwards and B.W. Barry, *Intl. J. Pharmaceutics*, **81**, R11–R14 (1992).]

or two wavenumber ranges, but using the same instrument. This does not occur with IR techniques and gives Raman spectroscopy a very big advantage particularly for geological or biogeological studies, where low-wavenumber bands can be quite definitive for sample identification and characterization. Such is the case for inorganic pigment analysis, where the ν(HgS), ν(PbO) and ν(SnS) modes, for example, all occur below 400 cm^{-1} and are inaccessible to most mid-IR spectrometers.[2] In the area of biological materials, too, Raman spectroscopy now finds considerable application in the characterization of real-world materials. Little or no sample preparation of a chemical or mechanical nature is necessary (an essential requirement for valuable art or archaeological specimens) and no desiccation is needed, as the Raman spectrum of water is weak and well characterized.[5] Hence, although IR spectroscopy has a recognizably greater sensitivity for the examination of proteins via the ν(CONH) amide I band near 1600 cm^{-1} because of the C=O band polarity, there is often much interference experienced in the IR spectra of natural proteinaceous materials through their natural hydration and the occurrence of water bending modes near 1600 cm^{-1}. The efficient absorption of IR radiation by wet or aqueous samples also diminishes the spectral quality of the absorption spectra of important biomaterials such as bone, skin, hair and collagen. In contrast, the Raman spectrum of human skin (Figure 3) is insensitive to the presence of water and the ν(CONH) band, although weaker than its IR counterpart, is clearly visible. Other features, such as lipoidal modes arising from the ν(C–C) in human skin, are better realized in the Raman spectra. The importance of water and of hydrogen bonding to biological systems can thus be directly accessed through Raman spectroscopic information and used to better define what may be happening in the cases where IR absorption measurements have been made on partially desiccated samples.

There now follows a brief compilation and discussion of important group frequencies in Raman spectra, the effect of adjacent groups, and some examples of how these have been used to good effect for the molecular characterization of diverse systems such as salt solutions, polymers, and inorganic pigments. Finally, some real-world Raman spectroscopic applications for identification of novel species, monitoring polymerization reactions, determining the geological composition of Martian meteorites, the characterization of valuable archaeological specimens, and biomedical diagnostics for diseased skin are described to illustrate the versatility of these techniques.

2 CHARACTERISTIC WAVENUMBERS OF RAMAN-ACTIVE MOLECULAR VIBRATIONS

Although the combined power of Raman and IR spectroscopic analysis for simple molecules has been demonstrated very effectively for innumerable cases in which molecular symmetry provides information on which theoretical predictions of structure can be based, the situation is less clear for molecular species of greater complexity that may have little or no symmetry over and above local considerations. Hence, the vibrational spectroscopic analysis of biologically relevant materials – enzymes, synthetic and biopolymers, and of large multi-ring systems – is reduced to that of the identification of group functionality rather than the overall molecular symmetry. However, it is possible to use Raman (and IR) spectroscopy to provide vital information about the structural changes that affect clearly identifiable groups and chemical moieties in a specimen. This is the basis of many important aspects of modern Raman spectroscopy, some of which are illustrated in this article, including the effect of chemical penetration enhancers for transdermal drug delivery systems on the keratotic and lipoidal components of human skin, as measured by the changes in band wavenumber position, band asymmetry,

This article was published in the *Handbook of Vibrational Spectroscopy* in 2006 by John Wiley & Sons, Ltd.
DOI: 10.1002/9780470027325.s4103

and bandwidths of the ν(CONH) amide I modes in the Raman spectrum. Similarly, the assessment of the effect of burial environment on archaeological biomaterials such as cotton, linen, bone, ivory and hair is dependent on information provided from Raman spectroscopy and that is again focused on particular group chemical functionalities such as phosphate, carbonate, glycosidic (COC) ring bands and the creation of unsaturation in long-chain aliphatic structures that are the targeted points for chain scission and subsequent molecular degradation.

Specific examples of current multidisciplinary research topics to illustrate these features will be provided; however, the key to the initial steps undertaken in the deductive Raman spectroscopic processes is the identification and assignment of vibrational wavenumber ranges that are characteristic of molecular group functionalities.

It must also be remembered that there are two major effects that are critical for the molecular dynamics of a vibrating system, namely, the electronic and mechanical contributions, which are dependent on bond strength and adjacent group substitution, collectively and individually. Hence, the useful interpretative information that can be deduced from the Raman spectra of molecular groupings or functionalities is typified in Table 1. Here, the bond strength effects on C–C, C–N and C–O band wavenumbers occasioned by an increase in bond multiplicity is clearly illustrated – a terminally coordinated carbon monoxide bond wavenumber of 2000 cm^{-1} in the Raman spectrum is reduced to about 1700 cm^{-1} for a ketonic feature and further reduced to about 1060 cm^{-1} for an alcohol ν(C–O) stretching mode. Similar progressions apply to the other important groups based on C–C and C–N bonds.

Table 1. Typical wavenumbers for the Raman-active bond stretching modes for C–N, C–O and C–C functionality.

Stretching mode	$\tilde{\nu}$ (cm^{-1})
$>$C—C$<$	1150
$>$C=C$<$	1630
—C≡C—	2130
$>$C—N$<$	1090
$>$C=N—	1670
—C≡N	2240
$>$C—O—	1060
$>$C=O	1700
←C≡O	2000

Another critical point to note is the presence of wavenumber *ranges* that are characteristic of most functional groups; often, practising spectroscopists will find that some ambiguity will arise in the assignment of molecular vibrations to band wavenumbers in Raman or IR spectra, which occurs because of the overlap of these characteristic spectral ranges. An example is provided in Section 3, in the form of an analysis of carbonyl group stretching modes that can occur within the wavenumber range 1600–1800 cm^{-1}. In this range, one would also expect to find vibrational modes arising from >C=N– >C=C<, and aromatic rings – hence, creating some possibilities of confusion in assignment. Resort to other spectroscopic information for the clarification of band assignments is then necessary, including band intensities and the adoption of comparison spectra of simplified model compounds. Further complications can arise when the system under investigation contains both inorganic and organic chemical groupings – such as in biodeterioration studies and, for example, in the Raman spectrum of ivory (Figure 4), which consists of collagen interspersed in a hydroxyapatite matrix.

Nevertheless, the tabulation of functional group vibrational assignment and wavenumber tables is an essential part of the Raman spectroscopist's armoury. There are exhaustive tabulations of vibrational group wavenumbers in the literature, some of these containing a wealth of fine detail; recently, there have appeared several databases and compilations of spectra, including one interactive, computerized database of molecular Raman spectra, the most useful of these being targeted at geology/mineralogy, polymer science and pigments.[6–9]

Table 2 provides a listing of the vibrational wavenumbers of the most important group functionalities in organic and inorganic chemistry; here, the most important vibrational modes, i.e. band stretching (ν), deformation (δ) and rocking (ρ), are described, as these represent probably the majority of the features used diagnostically in Raman spectroscopy. In Section 3, the influence of neighboring groups or substituents on the fundamental wavenumbers of selected bonds, namely C=C, C=O and C_6H_5– are described to indicate the diverse factors of an electronic, mass or geometric nature from which the wavenumber ranges of these important functionalities originate.

3 EFFECT OF ADJACENT GROUPS ON VIBRATIONAL WAVENUMBERS

It is undoubtedly true that the major source of difficulty in the application of vibrational spectroscopy to the

Handbook of Vibrational Spectroscopy, Online © 2006 John Wiley & Sons, Ltd.
This article is © 2006 John Wiley & Sons, Ltd.
This article was published in the *Handbook of Vibrational Spectroscopy* in 2006 by John Wiley & Sons, Ltd.
DOI: 10.1002/9780470027325.s4103

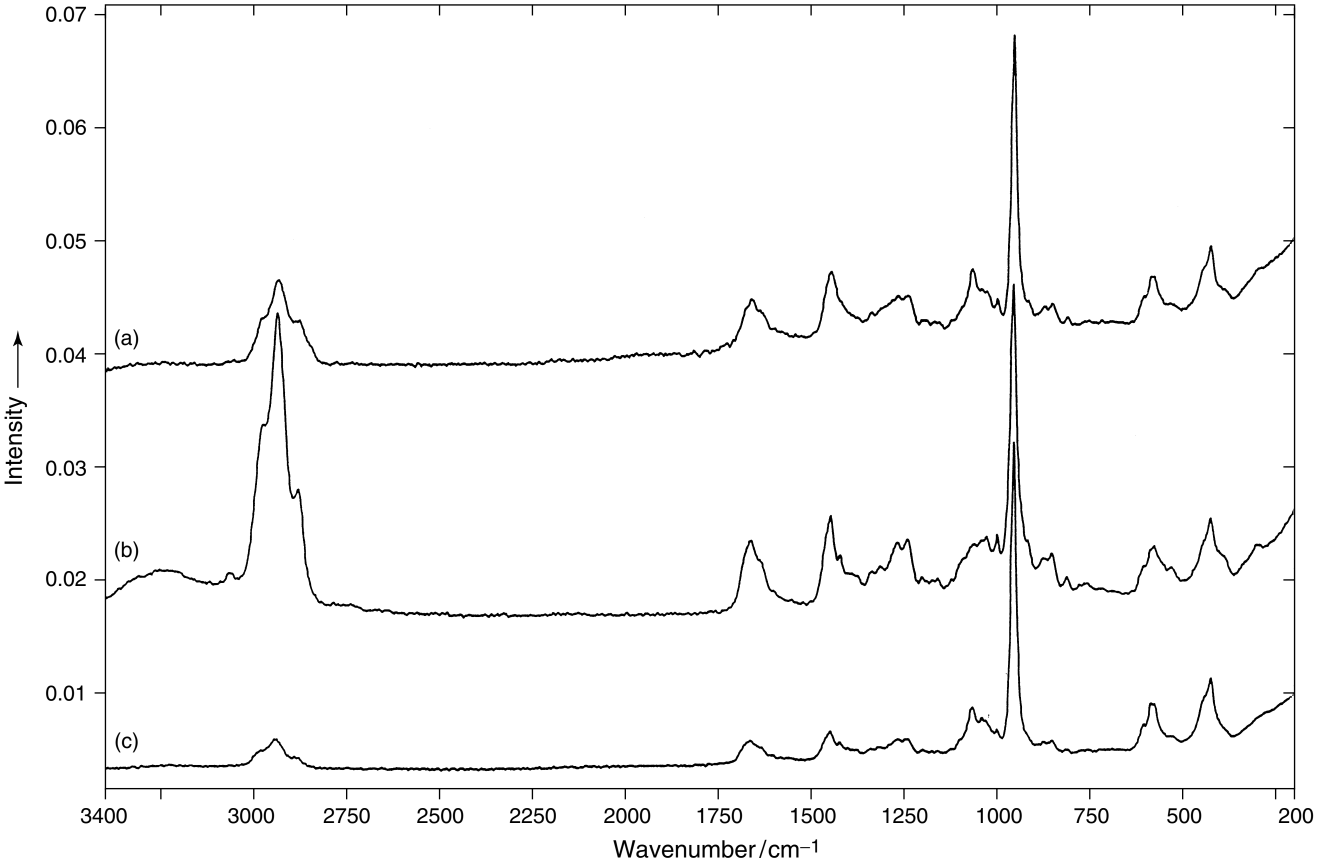

Figure 4. Raman spectrum of ivory – 1064 nm excitation, 500 scans, wavenumber range $\Delta\nu = 200{-}3400\,\mathrm{cm}^{-1}$. (a) Sperm whale, (b) elephant, (c) walrus. The strongest band at $960\,\mathrm{cm}^{-1}$ is the ν(PO) symmetric stretching of phosphate in the hydroxyapatite matrix. Weaker bands near 1440 and $1650\,\mathrm{cm}^{-1}$ are indicative of the $\delta(\mathrm{CH_2})$ and ν(CONH) amide I (α-helix) modes of collagen, respectively. Low-wavenumber bands near 450 and $600\,\mathrm{cm}^{-1}$ are assigned to phosphate $\delta(\mathrm{PO_2})$ deformations, which contain information about specimen crystallinities. [Reproduced with permission from Academic Press Inc., from H.G.M. Edwards, in "Encyclopaedia of Spectroscopy and Spectrometry", eds J.C. Lindon, G.E. Tranter and J.L. Holmes, Academic Press (1999).]

characterization and identification of molecular species arises in the assignment of spectral bands from functional groups or moieties; however, a correctly assigned spectrum contains a wealth of fine structural detail, which is there for interpretation. The range of vibrational wavenumbers offered by simple chemical groupings in different molecular environments is the root of the assignment problem and these can give rise to poor spectral interpretations or misassignments. Some classic examples of the origins and diversity of the observed wavenumbers for important chemical molecular functionalities are provided by the carbonyl (>C=O), alkene, (>C=C<), aromatic ring and disulfide bonding moieties.

3.1 Carbonyl bonds

Students and established practitioners of vibrational spectroscopy will at some time have encountered statements such as: "... carbonyl compounds have IR and Raman bands in the wavenumber region, $1900{-}1500\,\mathrm{cm}^{-1}$ ..."!

This spectral wavenumber range is one of the largest experienced in Raman spectroscopy and is shown diagrammatically in Figure 5 for $\mathrm{CH_3COX}$ molecules in which X = Cl and $\mathrm{N(CH_3)_2}$ occur at its extremes. Other important considerations also apply, such as the well-known intensity difference observed between carbonyl absorption in the IR and scattering in the Raman spectrum. In addition, where specific considerations of molecular symmetry apply, such as the case of an oxalate ion $\mathrm{C_2O_4}^{2-}$, the symmetric and antisymmetric ν(C=O) stretches are active in either the IR or Raman, but not in both.

3.1.1 Factors affecting carbonyl bond wavenumbers

The influence of electronic and neighboring group factors on the stretching wavenumber of the >C=O bond in carbonyls provides an excellent example of the complexity

This article was published in the *Handbook of Vibrational Spectroscopy* in 2006 by John Wiley & Sons, Ltd.
DOI: 10.1002/9780470027325.s4103

Table 2. Raman band wavenumber ranges for important organic chemical functionalities. [Reproduced in abridged form with permission of Academic Press Inc. from D. Lin-Vien, N.B. Colthup, W.G. Fateley and J.G. Grasselli, “Infrared and Raman Characteristic Frequencies of Organic Molecules”, Academic Press Inc., San Diego, USA (1991).]

Wavenumber range / cm^{-1}	Vibrational mode	Compound functionality
3400–3330	Antisymmetric NH_2 stretch	Primary amines
3380–3340	OH stretch	Aliphatic alcohols
3355–3325	Antisymmetric NH_2 stretch	Primary amides
3350–3300	NH stretch	Secondary amines
3335–3300	$C{\equiv}CH$ stretch	Alkyl acetylenes
3300–3250	Symmetric NH_2 stretch	Primary amines
3310–3290	NH stretch	Secondary amides
3190–3145	Symmetric NH_2 stretch	Primary amides
3100–3000	Aromatic CH stretch	Benzene derivatives
3095–3070	Antisymmetric $={CH_2}$ stretch	$C{=}CH_2$ derivatives
3062	CH stretch	Benzene
3057	Aromatic CH stretch	Alkyl benzenes
3040–3000	CH stretch	$C{=}CHR$ derivatives
3026	Symmetric $={CH_2}$ stretch	Ethylene (gas)
2990–2980	Symmetric $={CH_2}$ stretch	$C{=}CH_2$ derivatives
2969–2965	Antisymmetric CH_3 stretch	*n*-Alkanes
2929–2912	Antisymmetric CH_3 stretch	*n*-Alkanes
2884–2883	Symmetric CH_3 stretch	*n*-Alkanes
2861–2849	Symmetric CH_2 stretch	*n*-Alkanes
2850–2700	CHO group	Aliphatic aldehydes
2590–2560	SH stretch	Thiols
2316–2233	$C{\equiv}C$ stretch	$R{-}C{\equiv}C{-}CH_3$
2301–2231	$C{\equiv}C$ stretch	$R{-}C{\equiv}C{-}R'$
2300–2250	Pseudoantisymmetric $N{=}C{=}O$ stretch	Isocyanates
2161–2134	$N{\equiv}C$ stretch	Aliphatic isonitriles
2160–2100	$C{\equiv}C$ stretch	Alkyl alkynes
2156–2140	$C{\equiv}N$ stretch	Alkyl thiocyanates
1820	Symmetric $C{=}O$ stretch	Acetic anhydride
1810–1788	$C{=}O$ stretch	Acid halides
1805–1799	Symmetric $C{=}O$ stretch	Noncyclic anhydrides
1770–1730	$C{=}O$ stretch	Halogenated aldehydes
1743–1729	$C{=}O$ stretch	Cationic α-amino acids
1725–1700	$C{=}O$ stretch	Aliphatic ketones
1689–1644	$C{=}C$ stretch	Monofluoroalkenes
1686–1636	Amide I band	Primary amides (solids)
1680–1665	$C{=}C$ stretch	Tetraalkyl ethylenes
1678–1664	$C{=}C$ stretch	Trialkyl ethylenes
1676–1665	$C{=}C$ stretch	*trans*-Dialkyl ethylenes
1670–1630	Amide I band	Tertiary amides
1666–1652	$C{=}N$ stretch	Ketoximes
1665–1650	$C{=}N$ stretch	Semicarbazones
1663–1636	Symmetric $C{=}N$ stretch	Aldazines, ketazines
1660–1654	$C{=}C$ stretch	*cis*-Dialkyl ethylenes
1660–1650	Amide I band	Secondary amides
1660–1649	$C{=}N$ stretch	Aldoximes
1660–1610	$C{=}N$ stretch	Hydrazones
1658–1644	$C{=}C$ stretch	$R_2C{=}CH_2$
1654–1649	Symmetric $C{=}O$ stretch (cyclic dimer)	Carboxylic acids
1652–1642	$C{=}N$ stretch	Thiosemicarbazones
1650–1590	NH_2 scissors	Primary amines
1649–1625	$C{=}C$ stretch	Alkyl derivatives
1648–1640	$N{=}O$ stretch	Alkyl nitrites
1648–1638	$C{=}C$ stretch	$H_2C{=}CHR$
1634–1622	Antisymmetric NO_2 stretch	Alkyl nitrates

(*continued overleaf*)

Handbook of Vibrational Spectroscopy, Online © 2006 John Wiley & Sons, Ltd.

This article was published in the *Handbook of Vibrational Spectroscopy* in 2006 by John Wiley & Sons, Ltd.
DOI: 10.1002/9780470027325.s4103

Table 2. (*continued*)

Wavenumber range / cm^{-1}	Vibrational mode	Compound functionality
1630–1550	Ring stretches (doublet)	Benzene derivatives
1620–1540	Three or more coupled C=C stretches	Polyenes
1616–1571	C=C stretch	Chloroalkenes
1596–1547	C=C stretch	Bromoalkenes
1581–1465	C=C stretch	Iodoalkenes
1560–1550	Antisymmetric NO_2 stretch	Primary nitroalkanes
1555–1550	Antisymmetric NO_2 stretch	Secondary nitroalkanes
1545–1535	Antisymmetric NO_2 stretch	Tertiary nitroalkanes
1515–1490	Ring stretch	2-Furfuryl group
1480–1470	OCH_3, OCH_2 deformations	Aliphatic ethers
1473–1446	CH_3, OCH_2 deformations	*n*-Alkanes
1466–1465	CH_3 deformation	*n*-Alkanes
1450–1400	Pseudosymmetric N=C=O	Isocyanates
1443–1398	Ring stretch	2-Substituted thiophenes
1440–1340	Symmetric CO_2^- stretch	Carboxylate ions
1415–1400	Symmetric CO_2^- stretch	Dipolar and anionic α-amino acids
1415–1385	Ring stretch	Anthracenes
1395–1380	Symmetric NO_2 stretch	Primary nitroalkanes
1390–1370	Ring stretch	Naphthalenes
1385–1368	CH_3 symmetric deformation	*n*-Alkanes
1375–1360	Symmetric NO_2 stretch	Secondary nitroalkanes
1355–1345	Symmetric NO_2 stretch	Tertiary nitroalkanes
1350–1330	CH deformation	Isopropyl group
1320	Ring vibration	1,1-Dialkyl cyclopropanes
1314–1290	In-plane CH deformation	*trans*-Dialkyl ethylenes
1310–1250	Amide III band	Secondary amides
1310–1175	CH_2 twist and rock	*n*-Alkanes
1305–1295	CH_2 in-phase twist	*n*-Alkanes
1300–1280	CC bridge bond stretch	Biphenyls
1282–1275	Symmetric NO_2 stretch	Alkyl nitrates
1280–1240	Ring stretch	Epoxy derivatives
1270–1251	In-plane CH deformation	*cis*-Dialkyl ethylenes
1230–1200	Ring vibration	Paradisubstituted benzenes
1220–1200	Ring vibration	Mono- and 1,2-dialkyl cyclopanes
1205	C_6H_5–C vibration	Alkyl benzenes
1196–1188	Symmetric SO_2 stretch	Alkyl sulfates
1172–1165	Symmetric SO_2 stretch	Alkyl sulfonates
1150–950	CC stretches	*n*-Alkanes
1145–1125	Symmetric SO_2 stretch	Dialkyl sulfones
1130–1100	Symmetric C=C=C stretch	Allenes
1070–1040	S=O stretch	Aliphatic sulfoxides
1060–1020	Ring vibration	Orthodiubstituted benzenes
1040–990	Ring vibration	Pyrazoles
1030–1015	In-plane CH deformation	Monosubstituted benzenes
1030–1010	Trigonal ring breathing	3-Substituted pyridines
1030	Trigonal ring breathing	Pyridine
1029	Ring breathing	Trimethylene oxide
1010–990	Trigonal ring breathing	Mono-, meta-, and 1,3,5-substituted benzenes
1000–985	Trigonal ring breathing	2- and 4-Substituted pyridines
933	Ring vibration	Alkyl cyclobutanes
930–830	Symmetric COC stretch	Aliphatic ethers
905–837	CC skeletal stretch	*n*-Alkanes
900–890	Ring vibration	Alkyl cyclopentanes
900–850	Symmetric CNC stretch	Secondary amines
851–840	Pseudosymmetric CON stretch	*O*-Alkyl hydroxylamines
835–749	Skeletal stretch	Isopropyl group

DOI: 10.1002/9780470027325.s4103

Table 2. (*continued*)

Wavenumber range / cm^{-1}	Vibrational mode	Compound functionality
830–720	Ring vibration	Paradisubstuted benzenes
825–820	C_3O skeletal stretch	Secondary alcohols
818	Ring breathing	Tetrahydropyran
785–700	Ring vibration	Alkyl cyclohexanes
760–730	C_4O skeletal stretch	Tertiary alcohols
760–650	Symmetric skeletal stretch	*tert*-Butyl group
740–585	CS stretch (1 or more bands)	Alkyl sulfides
735–690	C=S stretch	Thiomades, thioureas (solid)
730–720	CCl stretch	Primary chloroalkanes
715–620	CS stretch	Dialkyl disulfides
690–650	Pseudosymmetric N=C=S	Alkyl isothiocyanates
660–650	CCl stretch, P_H conformation	Primary chloroalkanes
655–640	CBr stretch, P_c conformation	Primary bromoalkanes
630–615	Ring deformation	Monosubstituted benzenes
615–605	CCl stretch, S_{HH} conformation	Secondary chloroalkanes
610–590	Cl stretch, P_c conformation	Primary iodoalkanes
570–560	CCl stretch, T_{HHH} conformation	Tertiary chloroalkanes conformation
565–560	CBr stretch, P_H conformation	Primary bromoalkanes
540–535	CBr stretch, S_{HH} conformation	Secondary bromoalkanes
525–510	SS stretch	Dialkyl disulfides
520–510	CBr stretch, T_{HHH} conformation	Tertiary bromoalkanes
510–500	CI stretch, P_H conformation	Primary iodoalkanes
510–480	SS stretch	Dialkyl trisulfides
495–485	CI stretch, S_{HH} conformation	Secondary iodoalkanes
495–485	CI stretch, T_{HHH} conformation	Tertiary iodoalkanes
484–475	Skeletal deformation	Dialkyl dialkynes
425–150	Chain expansion	*n*-Alkanes
355–335	Skeletal deformation	Monoalkyl alkynes
200–160	Skeletal deformation	Aliphatic nitriles

and interrelationship of several effects, the results of which often do not correlate well with simplistic theoretical predictions; this is illustrated by the wavenumber change on substitution of H onto the carbon atom of the carbonyl in place of a carbon atom in aliphatic ketones, and the minimal effect of change of X in CX_3–C=O groups, contrary to the predictions of electronic theory.

3.1.2 Mass effects

The ν(C=O) stretching wavenumber is not sensitive to a mass change on the carbon atom, especially where the atoms are heavy. Atoms lighter than carbon, the most important being hydrogen, produce an effect that is similar in magnitude but in the opposite direction to that predicted on simple molecular dynamics. Hence, an aldehyde ν(C=O) occurs about 15 cm^{-1} higher than the corresponding ketone. Clearly, electronic effects are important, as exemplified by the ν(C=O) wavenumbers for acid halides and amides, where ν(–C(Cl)=O) is in the range 1810–1775 cm^{-1} (Raman medium weak, *mw*, intensity and polarized) and ν(–C(NH_2)=O) is in the range 1690–1640 cm^{-1} (Raman *mw* intensity and polarized), yet the NH_2 group is less than 50% of the mass of a Cl atom.

3.1.3 Bond geometry effects

Because of the high force constant for ν(C=O) stretching, which is approximately $1.8 \times 10^2\,N\,m^{-1}$, the movement of the X atoms in X_2C=O compounds transmitted through the C–X bonds affects the ν(C=O) but little. The interaction force constant $k_{cx,co}$, between the CX and CO bonds, changes as the internal bond angle changes, consequent upon geometry changes in cyclic carbonyls, and this affects the ν(C=O) wavenumber in a predictable way. For example, the wavenumber shifts in the ν(C=O) band relative to noncyclic carbonyl analogs for seven-to-four numbered ring structures are −8, +7, +37 and +76 cm^{-1}, respectively.

Of greater significance is the change in wavenumber of the ν(C=O) bond stretching consequent upon the geometry changes (and associated electronic environmental changes) of a carbonyl in one molecule in association with another group, which is often the carbonyl in another molecule

This article was published in the *Handbook of Vibrational Spectroscopy* in 2006 by John Wiley & Sons, Ltd.
DOI: 10.1002/9780470027325.s4103

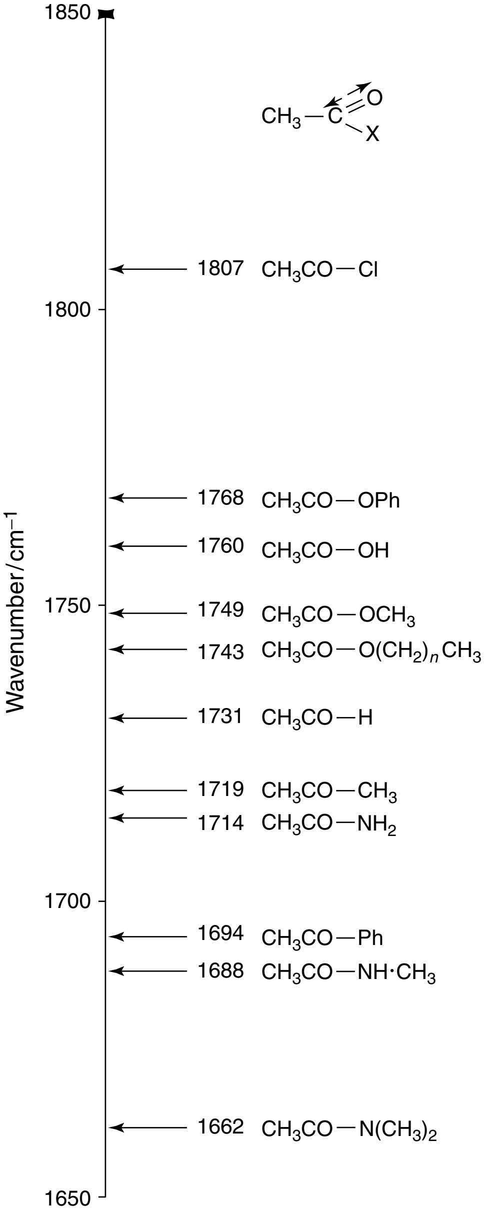

Figure 5. Wavenumber range of ν(C=O) vibrational modes in carbonyl compounds.

or the hydrogen atom in a hydrogen-bonded system. The contribution of Raman spectroscopy to the interpretation of molecular structures of associated molecules through a complex C=O band envelope will be illustrated later for polyacrylamides.

A further geometric effect that results in ν(C=O) bond wavenumber changes is provided by steric hindrance in molecules XYC=O, where X or Y are bulky groups. This will be considered below, as the most diverse and significant result of steric hindrance of the XYC grouping is demonstrated in a diminution of the conjugation of electronic effects between the C=O group and the X or Y atoms or groups.

3.1.4 Electronic effects

The polarity of the C=O group, exemplified by the resonance structure

$$X_2C{=}O \longleftrightarrow X_2C^{+}\text{–}O^{-}$$

contributes to a decrease in the bond strength and the C=O bond stretching force constant. If the atom or group X is electron attracting, this polar contribution to the C=O bond is reduced and the C=O wavenumber is increased; hence, ν(C=O) for an acid chloride, RC(Cl)=O, is about 1800 cm^{-1}, compared with about 1715 cm^{-1} for R$_2$C=O.

This effect is diminished with distance between the electron-attracting group and the C=O bond. Thus in an α-halocarbonyl

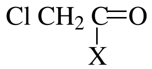

$$\mathrm{Cl\,CH_2\,\underset{\displaystyle X}{\underset{|}{C}}{=}O}$$

the ν(C=O) is now observed at ca. 1745 cm^{-1}, considerably less than the 1800 cm^{-1} observed for the acid chloride. However, a further fine point arises from the relative locations of the Cl and O atoms in the α-halocarbonyl, caused by internal rotation about the C–C bond. The dihedral angle Cl–C–C=O can be 0° (the cis conformer) or 120° (the gauche conformer) in two extremes – as the Cl is closer to the oxygen atom in the cis conformer this inhibits the ability of the oxygen to attract electrons relative to the gauche conformer. The ν(C=O) wavenumber in the cis conformer is +20 cm^{-1} relative to that of the gauche conformer.

A second electronic effect arises from mesomerism, in which the nonbonding electrons of an atom attached to the carbon atom of the carbonyl bond can be made available for donation of electrons to the oxygen atom of the carbonyl:

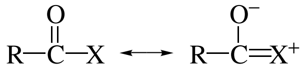

$$\mathrm{R{-}\overset{\displaystyle O}{\overset{\|}{C}}{-}X} \longleftrightarrow \mathrm{R{-}\overset{\displaystyle O^{-}}{\overset{|}{C}}{=}X^{+}}$$

The result is a weakening of the ν(C=O) force constant and a strengthening of the ν(C–X) force constant. The effect is insignificant for acid chlorides because of the poor electron-donating effect in Cl atoms, hence ν(C=O) in RCOCl is near 1800 cm^{-1}; however, where X is OR as in an ester, the ν(C=O) is lowered to about 1740 cm^{-1} from this effect. In an amide, where X is –NH$_2$, this effect is most significant and contributes largely to the low value of the observed ν(C=O) between 1640 and 1665 cm^{-1}.

In more complex molecules, the electron-donating power of X can be diminished by bonding with other electron-attracting groups such as a chlorine atom in a chloroformate (ν(C=O) ca. 1780 cm^{-1}) or an unsaturated ester such as vinyl acetate (ethanoate; ν(C=O) ca. 1770 cm^{-1}).

This article was published in the *Handbook of Vibrational Spectroscopy* in 2006 by John Wiley & Sons, Ltd.
DOI: 10.1002/9780470027325.s4103

The third most significant electron effect is that of conjugation, in which the double-bond character of the C=O is reduced, exemplified by contributions of the type

$$O{=}C{-}C{=}C \longleftrightarrow {}^{-}O{-}C{=}C{-}C^{+}$$

and can be enhanced if there is an OH or NH group on the β-unsaturated carbon atom that can additionally hydrogen bond to the C=O in the form

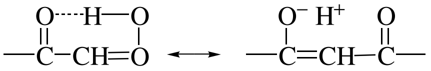

$$\overset{O\cdots H-O}{\overset{\| \qquad\quad |}{-C-CH=O}} \longleftrightarrow \overset{O^{-}\ H^{+}\qquad O}{\overset{| \qquad\qquad\quad \|}{-C=CH-C-}}$$

An example of this is provided in the enolization of molecular species such as acetyl acetone (2,4-pentadione):

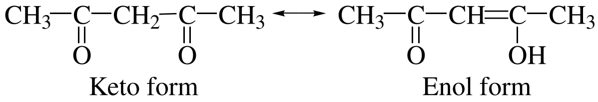

$$CH_3-\underset{\underset{O}{\|}}{C}-CH_2-\underset{\underset{O}{\|}}{C}-CH_3 \longleftrightarrow CH_3-\underset{\underset{O}{\|}}{C}-CH=\underset{\underset{OH}{|}}{C}-CH_3$$

Here, the ν(CO) wavenumber of the keto–enol tautomers is reduced to near 1600 cm^{-1}. It is in this context that the geometric consideration of the coplanarity of the C=O and the rest of the molecule becomes important, because in the coplanar configuration there is greatest overlap of π electrons between the C=C and C=O moieties. For example, acetophenone (coplanar groups) has a ν(C=O) of 1685 cm^{-1}, whereas 2,6-dimethylacetophenone (nonplanar groups) has a ν(C=O) at 1705 cm^{-1}.

3.2 Alkenes

The Raman spectra of alkenes have been well studied. This reflects the importance of the >C=C< moiety in processes of industrial interest, its relevance as a site for carbon-chain scission in reactions particularly involving environmental biodeterioration, and its presence in natural products as a conjugated group in carotenoids and in plant resins based on the diterpene, abietic acid. The presence of the ν(C=C) stretching mode as a strong band near 1650 cm^{-1} makes it a useful Raman marker. The Raman wavenumbers of 75 hydrocarbon alkenes have been reported[10] and form the basis of modern band assignments and wavenumber ranges. In contrast, the IR activity of the >C=C< mode is less well characterized and the bands are often of weak intensity and symmetry forbidden. The >C=C< group vibration in hydrocarbons and in substituted alkenes where the local symmetry is centrosymmetric, as in *trans*-dihalo alkenes, is strictly forbidden in the IR, but nevertheless the ν(C=C) mode is sometimes observed as a very weak band in the IR.

A table of ν(C=C) wavenumbers in simple alkenes based on ethene with methyl substituents is given in Table 3. Although the wavenumber range is significantly smaller than that observed for carbonyls, nevertheless similar considerations relating to the mass and electronic properties of the substituents still apply for the series of methylethenes considered here. As in the case of the >C=O< moiety, the >C=C< stretching mode also has a high stretching force constant, which is not significantly affected by the C–C force constants of adjacent methyl substituents (Table 3). Hence, although the ν(C=C) in ethene occurs at 1623 cm^{-1}, the corresponding mode in tetramethylethene occurs at 1670 cm^{-1} despite the significant increase in mass of the vibrating system of nearly 400%! Again, this increase in ν(C=C) wavenumber from ethene to tetramethylethene reflects the important contribution of the electron-donating methyl groups to the >C=C< bond strength, and this is seen additionally to result in a progressive increase in ν(C=C) from 1623 cm^{-1} in ethene to 1640, 1652 (average), 1660 and 1670 cm^{-1} for the mono-, di-, tri-, and tetramethyl compounds, respectively.

Table 3. Effect of substitution on the wavenumbers of ν(C=C) stretching in the Raman spectra of alkenes.

Molecule	$\tilde{\nu}$ (C=C) (cm^{-1})
$CH_2{=}CH_2$	1623
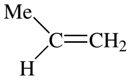	1640
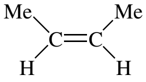 cis	1644
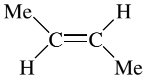 trans	1662
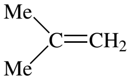	1650
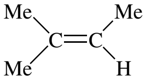	1660
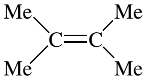	1670

A very useful Raman diagnostic marker for structural studies is provided by the change in wavenumbers of the ν(C=C) with local symmetry and conformation changes for the disubstituted ethenes. Here, the trans conformer has the highest observed wavenumber at 1662 cm^{-1}, followed

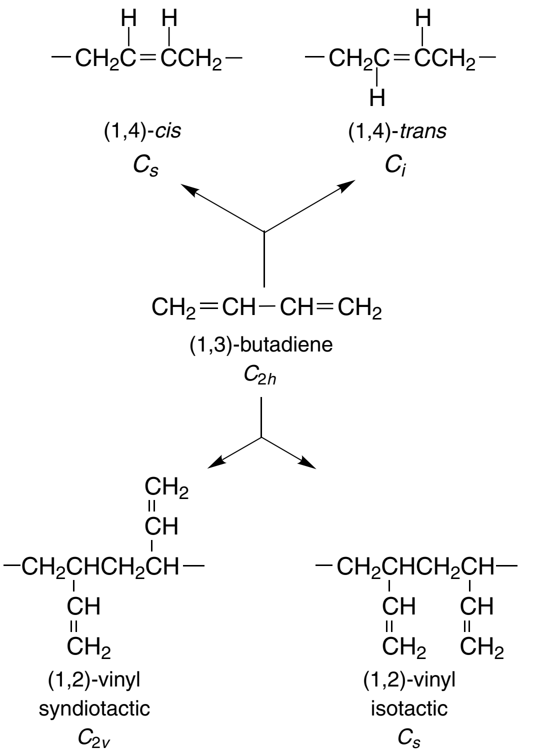

Figure 6. Reaction schemes for the living anionic polymerization of 1,3-butadiene to cis, trans and vinyl polybutadienes. Local molecular symmetry point groups are also shown. [Reproduced with permission of Butterworth-Heinemann from S. Poshyachinda, H.G.M. Edwards and A.F. Johnson, *Polymer*, **32**, 334–337 (1991).]

by the pendant vinylic conformer at $1650\,cm^{-1}$ and the cis conformer at $1644\,cm^{-1}$. This diagnostic property has been used to good effect in the application of Raman spectroscopy to the analysis of polyenes, such as polyisoprene and polybutadiene. Figure 6 shows a scheme for the polymerization of buta-1-3-diene, which is accomplished industrially using butyllithium initiator in an aprotic solvent. The reaction is known as "living anionic polymerization" and can be terminated with precipitation of the polymer by addition of alcohol or continued by addition and polymerization of another diene. Generally, a mixture of all three conformers is obtained, but selectivity of the reaction conditions assisted by Raman spectroscopic monitoring procedures based on the quantitative band analysis of the $1600–1680\,cm^{-1}$ region can be used to produce polymers with the desired conformational microstructures. Examples of the commercially important diblock polybutadienes (PBB), with block A consisting of 1,3-butadiene monomer addition, and block B 1,2-butadiene monomer addition, is shown in Figure 7. From this spectral stack-plot, it is clear that Raman spectroscopy can provide useful quantitative diagnostic structural information in an industrial polymerization process. By monitoring the monomer

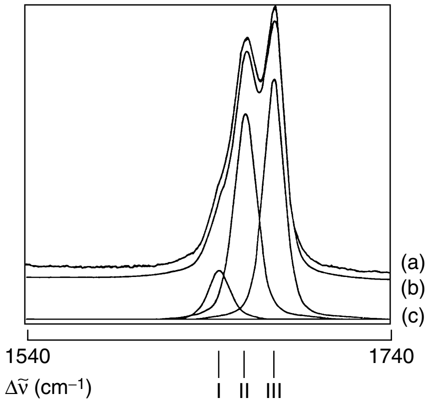

Raman spectrum of first-stage polymerization of butadiene, $\Delta\tilde{\nu}=1540–1740\,cm^{-1}$: (a) observed spectrum; (b) computer calculated; (c) resolved spectrum; I (1,2)-vinyl, II (1.4)-*cis*, III (1,4)-*trans* polybutadiene. Calculated composition: I (9.6%), II (43.8%) and III (46.6%).

(a)

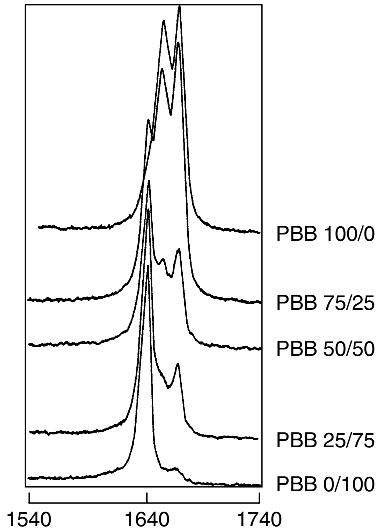

Microstructure determination of diblock polybutadienes; Raman spectra, $\Delta\tilde{\nu}=1540–1740\,cm^{-1}$ for PBB 100/0, 75/25, 50/50, 25/75 and 0/100 compositions.

Percentage microstructure of the diblock polymers

Sample	First block			Second block		
	vinyl	cis	trans	vinyl	cis	trans
PBB 0/100	–	–	–	94.2	0.0	5.8
PBB 25/75	9.6	43.8	46.6	94.0	0.4	5.6
PBB 50/50	9.5	43.3	47.2	94.1	0.0	5.9
PBB 75/25	9.3	44.3	46.4	94.4	0.2	5.4
PBB 100/0	9.9	43.5	46.4	–	–	–

(b)

Figure 7. Stack-plot Raman spectra of first-stage polymerization of 1,3-butadiene, 1064 nm excitation, $\Delta\nu = 1540–1740\,cm^{-1}$, the ν(C=C) stretching region. (a) Observed Raman spectra and computer-calculated spectra with resolved components. (b) Microstructural determination of diblock PBB, same ν(C=C) region, with compositional data for the first and second blocks. [Reproduced with permission of Butterworth-Heinemann from S. Poshyachinda, H.G.M. Edwards and A.F. Johnson, *Polymer*, **32**, 334–337 (1991).]

This article was published in the *Handbook of Vibrational Spectroscopy* in 2006 by John Wiley & Sons, Ltd.
DOI: 10.1002/9780470027325.s4103

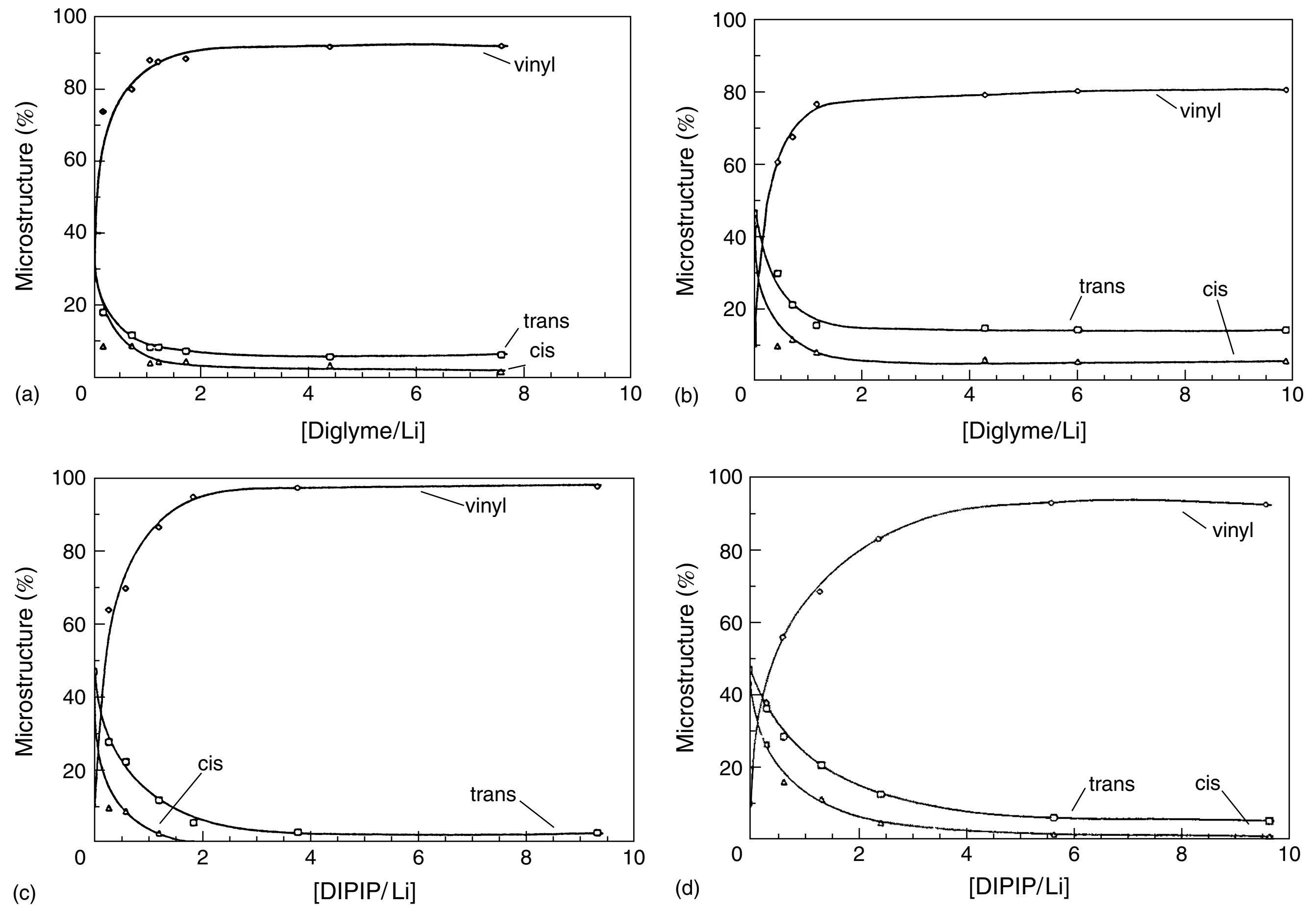

Figure 8. Plots of composition of synthetic polybutadienes against initiator concentration based on quantitative Raman spectroscopic measurements of the $\nu(C{=}C)$ band composition in the wavenumber range 1540–1740 cm^{-1}: (a) diglyme/*n*-BuLi at 0 °C; (b) diglyme/*n*-BuLi at 30 °C. (c) DIPIP/*n*-BuLi at 0 °C; (d) DIPIP/*n*-BuLi at 30 °C. Raman structural-spectral data of this type have provided unique information from nondestructive and rapid characterization of polymer compositions that have facilitated the tailoring of materials with specific microstructures. [Reproduced with permission of Butterworth-Heinemann from S. Poshyachinida, H.G.M. Edwards and A.F. Johnson, *Polymer*, **32**, 338–342 (1991).]

species consumption or the $\nu(C{=}C)$ band in a particular conformer as a function of temperature, solvent, initiator concentration and time, it is possible using the Raman spectrum to select the conditions for controlling the reaction pathway. An example is given in the plot in Figure 8, which gives some Raman spectroscopic measurements of high-vinyl polymerization, i.e. 1-2-diene addition, a desirable polymeric product for automotive industrial applications. The presence of the $\nu(C{=}C)$ bands from all three possible butadiene conformers in the Raman spectrum is very useful; the trans conformer is centrosymmetric and the $\nu(C{=}C)$ mode does not occur in the IR spectrum.[11]

Finally, conjugation of the >C=C< bond with other functionality results in wavenumber changes in both groups. It is interesting to examine the effect of conjugation (Figure 9) of a >C=O group with a >C=C in acrylaldehyde, where the $\nu(C{=}O)$ is decreased from 1725 to 1703 cm^{-1} and the $\nu(C{=}C)$ is decreased from 1640

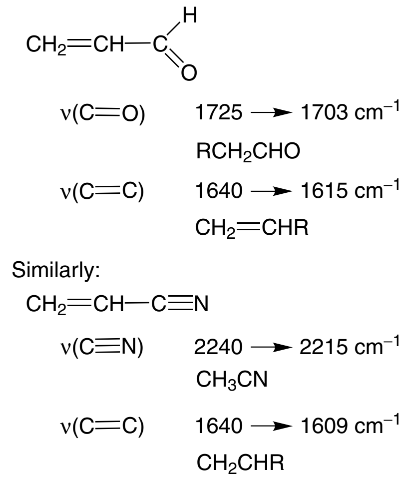

Figure 9. Conjugation of $\nu(C{=}C)$ and $\nu(C{=}O)$ illustrating the effects of neighboring group participation on the observed wavenumbers of stretching bands.

DOI: 10.1002/9780470027325.s4103

to 1615 cm^{-1} compared with the parent aldehydes and alkenes. Similarly, the conjugation of a nitrile group with an alkene group results in a decrease of the ν(C≡N) from 2240 to 2215 cm^{-1} compared with acetonitrile and the ν(C=C) reduce from 1640 to 1609 cm^{-1} compared with propene. The explanation of this reduction in wavenumber of both C=C and C=O and C≡N functionalities is that the linking C–C bond is strengthened by the delocalization of electronic charge over the four-atom systems, either C=C–C=O or C=C–C≡N.

An interesting observation of the ν(C=C) mode in the Raman spectra of conjugated >C=C< compounds is provided by the work of Veronelli *et al.*[12] on a series of naturally occurring carotenoids from birds' feathers. The conjugated moiety is now (–C=C–C=C–) and two Raman bands are observed near 1520 cm^{-1} (characteristic of the >C=C< mode) and 1150 cm^{-1} (characteristic of the >C–C< mode). In several papers dealing with the application of Raman spectroscopy to the in situ characterization of key molecular biomarkers in chemical encrustations produced by lichens under stressed environmental biogeological conditions, Edwards *et al.*[13] have observed the presence of β-carotene in lichens growing in stressed Antarctic environments (Figure 10); the two carotenoid features at 1523 and 1157 cm^{-1} are clearly seen in these spectra.

Although Raman spectra have been used successfully in the determination of the structures of alkenes, and substituted and conjugated alkenes, the situation does not apply equally in all cases. Hence, although the Raman literature contains a good database of some 30 or more allyl compounds (which approximate to monoalkyl ethenes in structure), the CH_2=CH–CH_2X grouping does not yield definitive conformational evidence based on the analysis of the strong Raman band arising from ν(C=C) stretching in the 1625–1650 cm^{-1} region. Rotational conformational studies are complicated by the existence of isomers based on gauche structures in addition to the cis and trans conformers discussed earlier for butadienes; for example, the ν(C=C) of the gauche isomer for allyl chloride is larger than for the cis conformer, but the effect is the other way round for the allyl amines. In other cases, the cis and gauche conformers are not resolved, such as for allyl cyanide.

3.3 Groups containing sulfur: disulfide bridges

The groups S–H, C–S and S–O are important in experiments involving the spectroscopic detection and monitoring of synthetic and natural sulfur compounds. Whereas the S–O groups are strongly polar and exhibit strong IR absorptions, the less polar S–H and C–S bonds are normally very

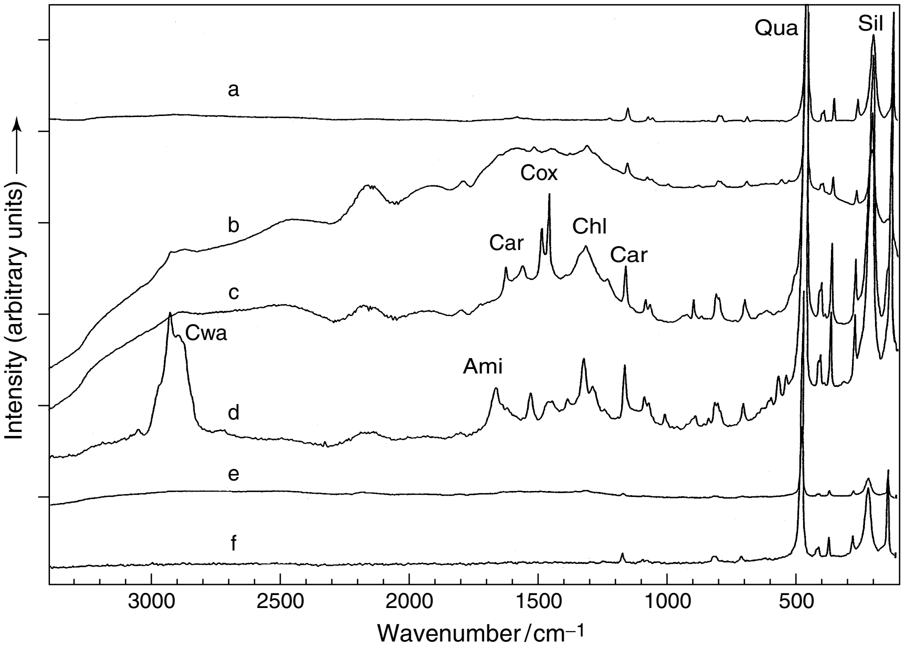

Figure 10. Raman microscope spectral (1064 nm excitation) stack-plot of a cryptoendolithic lichen colony in an environmentally stressed habitat, East Beacon sandstone, Victoria Land, Antarctica. The spectra (a)–(f) represent different zones of occupation through a 10-mm vertical section of rock from the outer surface (quartz, Fe_2O_3) through the fungal and lichen layers (b, c and d) to the inner substrate rock (e and f). Key structural features are identified and some are labelled in the stack-plotted spectra, including quartz (Qua) chlorophyll (Chl), β-carotene (Car), calcium oxalate (Cox), amide (Ami) and cell wall material (Cwa). [Reproduced with permission of N.C. Russell, H.G.M. Edwards, D.D. Wynn-Williams, *Antarctic Science*, **10**, 63–74 (1998).]

This article was published in the *Handbook of Vibrational Spectroscopy* in 2006 by John Wiley & Sons, Ltd.
DOI: 10.1002/9780470027325.s4103

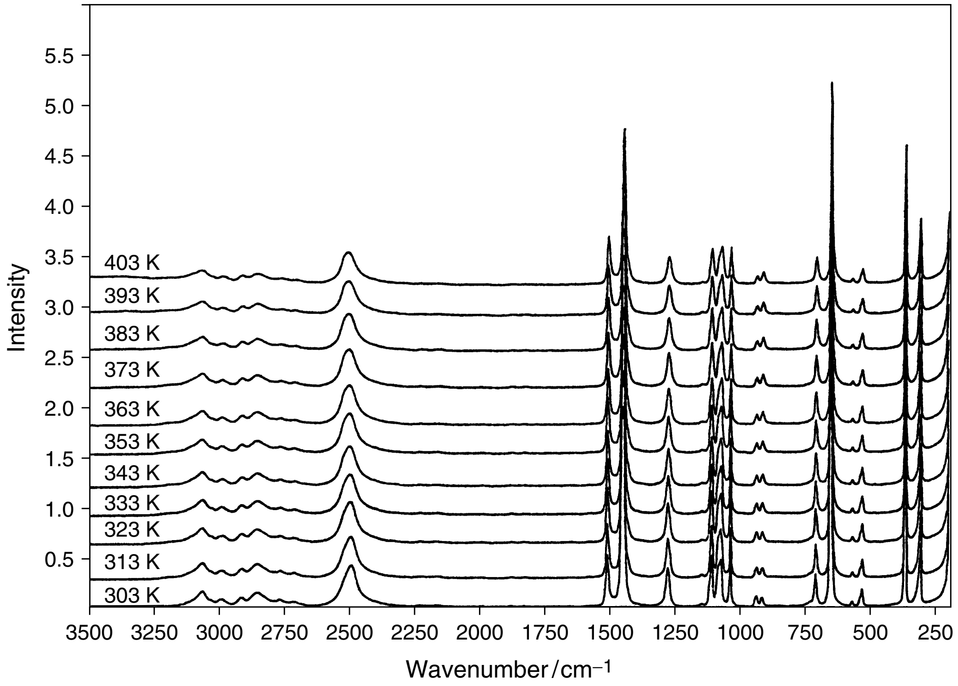

Figure 11. Raman spectra of 2,5-dimercapto-1,3,4-thiadiazole (DMTD), 1064 nm excitation, wavenumber range $\Delta\nu = 200-3500\,\mathrm{cm}^{-1}$, temperature range 303–403 K. The broad, asymmetric ν(S–H) stretching band at $\sim 2500\,\mathrm{cm}^{-1}$ can be resolved into two components, at 2519 and $2485\,\mathrm{cm}^{-1}$ assigned to free and to hydrogen-bonded SH modes, respectively. The low-intensity doublet near $940\,\mathrm{cm}^{-1}$ consists of vibrational modes due to the δ(C–SH) deformation at 940 and $919\,\mathrm{cm}^{-1}$, for the hydrogen-bonded and free molecular species, respectively. [Reproduced with permission from E.E. Lawson, H.G.M. Edwards and A.F. Johnson, *J. Raman Spectroscopy*, **26**, 617–622 (1995); copyright J. Wiley & Sons, Ltd.]

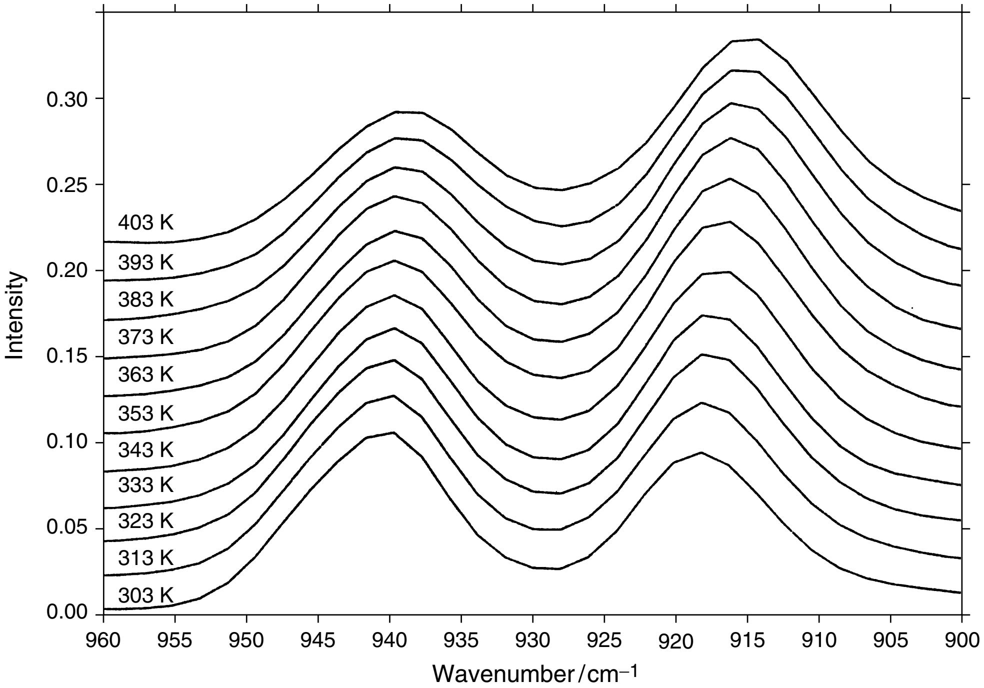

Figure 12. Wavenumber expanded region, $900-960\,\mathrm{cm}^{-1}$, of the Raman spectrum of DMTD over the temperature range 303–403 K at intervals of 10 ± 1 K. Note the relative intensity changes between the δ(CSH) modes at 940 and $919\,\mathrm{cm}^{-1}$ – the longer wavenumber mode assigned to the hydrogen-bonded species decreases in intensity relative to that at shorter wavenumber with increase in temperature, reflecting the thermal instability of the intermolecular hydrogen bonds. [Reproduced with permission of E.E. Lawson, H.G.M. Edwards and A.F. Johnson, *J. Raman Spectroscopy*, **26**, 617–622 (1995); copyright J. Wiley & Sons, Ltd.]

DOI: 10.1002/9780470027325.s4103

weak in IR spectra. Hence, hydrogen-bonding studies of thiols are usually undertaken using the Raman technique; an example of the study of ν(S–H) bonding by Raman spectroscopy as a function of temperature is shown in Figure 11, from which important quantitative thermodynamic information is obtained.[14]

An expanded wavenumber stack-plot of the Raman spectra of the δ(CSH) deformation region of DMTD is shown in Figure 12; the longer wavenumber band of the doublet at 940 cm^{-1} is assigned to the hydrogen-bonded molecules, whereas the feature at 919 cm^{-1} is the corresponding mode for the free, unbound species. Quantitative Raman spectroscopic measurements on these two bands as a function of temperature in the range 303–403 K at intervals of 10 ± 1 K have yielded information about the equilibrium

$$[\text{free}] \xrightleftharpoons{K_\text{c}} [\text{bound}]$$

where

$$K_\text{c} = \frac{(\text{intensity of } 940\,\text{cm}^{-1})}{(\text{intensity of } 919\,\text{cm}^{-1})}$$

As $\Delta G^\circ = -RT \ln K_\text{c}$ and $\ln K_\text{c} = -\Delta H^\circ/RT + S^\circ/R$, then the gradient of a plot of $\ln K_\text{c}$ against $1/T$ (Figure 13) gives the average enthalpy for formation of a hydrogen bond in DMTD over this temperature range as $-3.35 \pm \text{kJ mol}^{-1}$ and $\Delta S^\circ = -12\,\text{kJ mol}^{-1}$.

However, it is perhaps more significant to discuss here the Raman spectroscopy of ν(–S–S–) disulfide bridging groups, which, because of their nonpolarity and symmetry, do not exhibit an IR absorption spectrum. Hence, information about this important biological structural entity is provided from Raman spectroscopic studies. The –S–S– group has a highly significant presence in biomolecular diagnostics since it forms the bonding group between cysteine amino acid (Cys) residues and its scission is indicative of degradation of keratotic materials, which occurs widely in diverse natural biopolymers including skin, hair, claws, beaks, feathers, horn, hoof, reptilian scales, and shells. Although the composition of animal and human keratotics varies from about 1% to 10% cysteine, the onset of chemical or natural degradation is manifest by a decrease in intensity of the ν(S–S) modes in the region of 490–520 cm^{-1}; the ν(S–S) modes are normally observed in the Raman spectrum as a rather broad, asymmetric feature as generally there are several conformations of the C–S–S–C moiety present. Figure 14 shows some important conformers based on the classic work of Qian and Krimm on the –S–S– band and cis–trans, or gauche structures; the CSSC grouping is hence described correctly as a tgt, ggt or ggg type structure, where g and t are gauche and trans structures, respectively.[15] Application of Raman spectroscopy to the complex, real-world structures of diseased human skin, chemically bleached hair, archaeological provenancing of animal horn and hoof and the characterization of reptilian skins for pharmaceutical and drug disposition studies have followed, for which the observation of the ν(S–S) modes is a vital part of the procedure.[16] Figure 15 shows an example of the stack-plot of the FT Raman spectra of hoof, horn, and

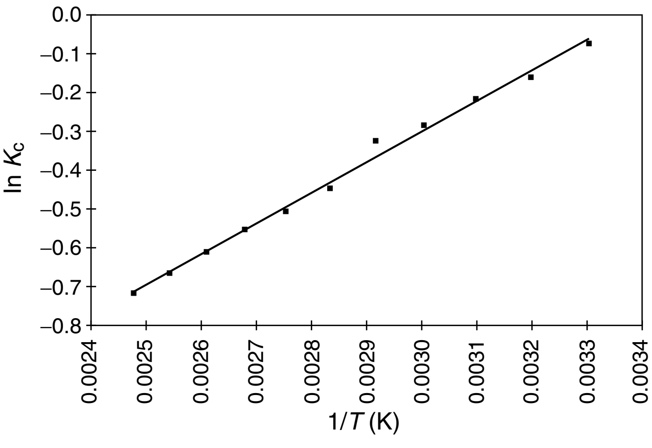

Figure 13. Plot of $\ln K_\text{c}$ against $1/T$ for DMTD based on the Raman spectra recorded of the free and hydrogen-bonded δ(CSH) modes over the temperature range 303–403 K. From this plot the ΔH° and ΔS° thermodynamic parameters for the formation of hydrogen bonds can be evaluated for DMTD. [Reproduced with permission of E.E. Lawson, H.G.M. Edwards and A.F. Johnson, *J. Raman Spectroscopy*, **26**, 617–622 (1995); copyright J. Wiley & Sons, Ltd.]

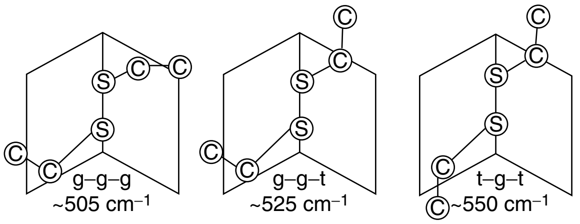

ν(S—S) wavenumbers and conformational dependence for cystine residues.

Residue	Group	Wavenumber /cm^{-1}	Assignment
Cys	S—S	540	trans–gauche–trans
		525	gauche–gauche–trans
		510	gauche–gauche–gauche
	C—S	745–700	trans
		670–630	gauche

Figure 14. Arrangement of atoms in disulfide bridges of gauche and trans conformations of the –CSSC– linkage. The Raman-active ν(S–S) wavenumbers for these conformations are given below. [Reproduced with permission of Elsevier Science Ltd., from H.G.M. Edwards, D.E. Hunt and M.G. Sibley, *Spectrochimica Acta Part A*, **54**, 745–747 (1998).]

This article was published in the *Handbook of Vibrational Spectroscopy* in 2006 by John Wiley & Sons, Ltd.
DOI: 10.1002/9780470027325.s4103

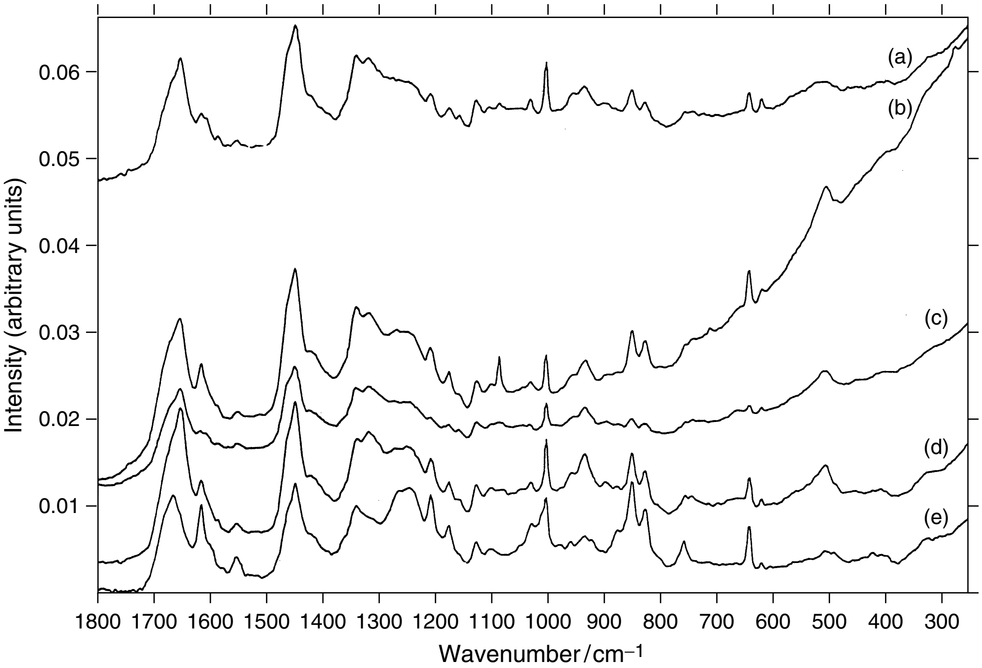

Figure 15. Fourier transform Raman spectral stack-plot of natural keratotic biomaterials, wavenumber range 250–1800 cm^{-1}, 1064 nm excitation: (a) hoof, (b) kudu horn, (c) human nail, (d) Texas longhorn, (e) tortoiseshell. Although spectroscopically each keratotic biopolymer is easily recognizable generally as such from its Raman spectrum, the subtle changes in the ν(S–S) and ν(C–S) regions particularly afford a method for differentiation of the specimens. [Reproduced with permission of Elsevier Science from H.G.M. Edwards, D.E. Hunt and M.G. Sibley, *Spectrochimica Acta, Part A*, **54**, 745–757 (1998).]

tortoiseshell, all of which exhibit prominent, broad ν(S–S) bands that can be used for the archaeological study of their environmental biodeterioration.

Although the Raman spectra of these keratotic biopolymers are complex and contain many bands in the functionality region (Figure 15), all features discernible in the spectra are assignable from databases of model compounds; this provides an excellent example of the power of spectral-structural correlations in Raman spectroscopy for the characterization of complex molecular materials and for which a start is provided by listings of wavenumbers such as those given in Table 2. The value of comprehensive wavenumber assignment tables such as that provided in Table 4 is apparent from the recent applications of Raman spectroscopy to biomedical diagnostics, especially for the detection of diseased skin and body organs. In this way, there has been a novel approach to the understanding of cancerous tumors and their therapeutic treatment provided by Raman spectroscopic techniques, in vivo and in vitro.[17]

3.4 Aromatic ring vibrations

The Raman spectra of benzene derivatives have been studied extensively; there is a tendency to regard the strong Raman-active symmetric ν(C–C) mode, the so-called ring-breathing vibration, that occurs near 1000 cm^{-1} in some benzene compounds as the definitive characteristic Raman spectral mode of aromatic compounds generally. This is only partially correct as Figure 16 will demonstrate; here, the Raman spectra of 4-toluenesulfonic acid (p-TsOH) and benzene sulfonic acid are stack-plotted. The feature at 1003 cm^{-1} in the benzene sulfonic acid spectrum, assigned to the ring-breathing ν(C–C) mode, occurs only very weakly in p-TsOH. Hence, it is not a characteristic feature of the aromatic ring but, as will be seen later, it is more indicative of a substituted benzene ring that does *not* contain para substituents. Hence, in the Raman spectrum of human skin, a complex biopolymer, which can be broadly described as a mixture of components of water, keratins (proteins) and lipids (fats), the sharp feature at 1003 cm^{-1} is indicative of the phenylalanine amino acid residue in the proteinaceous component.

It is useful here to consider in some more detail the Raman-active bands of benzenoid aromatic compounds. The first point to make is the complexity of the situation – a monosubstituted benzene ring, such as that of chlorobenzene, has a total of 30 vibrational modes, which are shown diagrammatically in Figure 17. It is important to realize that most of these modes involving predominantly C–C or C–H motion do not change with the substitution of X in C_6H_5X, and only six of the vibrational modes shown in Figure 17 are substituent sensitive.[18]

Table 4. Examples of comprehensive Raman spectra assignments for complex biopolymers – naturally occurring keratins. [Reproduced with permission of Elsevier Science; H.G.M. Edwards, D.E. Hunt and M.G. Sibley, *Spectrochimica Acta, Part A*, **54**, 745–757 (1998).]

Assignments for keratin samples[a]						Approximate assignment
Bovine keratin	Bovine hoof	Texas longhorn	Kudu horn	Tortoiseshell	Human nail	
3264 wbr	3260 wbr	3258 wbr	3256 wbr	3262 wbr	3263 wbr	ν(NH) symmetric stretch
3059 w	3061 w	3061 w	3061 w	3060 w	3061 w	ν(CH) alkenic
2960 ssh	2963 ssh	2964 ssh	2962 ssh	2964 ssh	2960 ssh	ν(CH$_3$) antisymmetric
2931 vs	2930 vs	2932 vs	2930 vs	2931 vs	2930 vs	ν(CH$_3$) symmetric
2875 ssh	2873 ssh	2877 ssh	2878 ssh	2874 ssh	2876 ssh	ν(CH$_2$) symmetric
2765 vw		2764 vw	2762 vw			ν(CH) aliphatic
2725 vw		2727 vw	2726 vw		2726 vw	ν(CH) aliphatic
1670 ssh	1670 ssh	1668 ssh	1672 ssh	1666 s	1670 msh	ν(CO) amide I; β-sheet
1653 s	1653 s	1652 s	1652 s		1652 m	ν(CO) amide I; α-helix
1615 m	1614 m	1615 m	1615 m	1615 s	1615 w	ν(CC) alkenic
1605 msh	1606 msh	1605 m			1606 w	ν(CC) alkenic
1585 w	1585 w	1584 w	1587 w	1586 wsh	1585 w	ν(CC) alkenic
1550 w	1550 vw	1552 vw	1550 w	1552 w	1550 w	δ(NH); ν(CN)
				1531 vvw		δ(NH)
1518 vw	1513 vvw			1516 vvw		ν(CC)
1460 msh	1456 ssh	1461 ssh	1461 msh		1460 msh	ν(CH$_2$) deformation
1448 s	1448 s	1448 s	1448 s	1448 s	1448 s	δ(CH$_2$) scissoring
1419 mwbrsh	1421 mwbrsh	1419 mwbrsh	1418 msbrsh	1421 mbrsh	1420 mwbrsh	δ(CH$_3$) deformation
1340 m	1338 m	1338 m	1338 mw	1338 m	1339 m	δ(CH$_2$) deformation
1317 m	1317 m	1317 m	1317 mw	1318 msh	1315 m	δ(CH$_2$) deformation
1282 m	1280 vvw	1279 wsh	1278 mw		1280 w	ν(CN); δ(NH) amide III α-helix
				1262 ms		ν(CN); δ(NH) amide III α-helix
1243 m	1245 vvw	1249 m	1245 m	1245 s	1245 w	δ(CH$_2$) wagging; v(CN) amide III
1207 w	1207 w	1206 w	1207 w	1206 s	1206 vw	ν(CC)
1174 w	1174 w	1173 w	1176 vw	1173 m	1174 vw	ν(CC)
1155 vw	1155 w	1154 vw	1156 vw		1156 vw	ν(CC), δ(OH)
1124 w	1126 w	1126 vw	1125 vw	1125 w	1127 vw	ν(CC) skeletal, trans conformation
1100 vw	1102 vw	1101 vw	1101vvw	1101 vw	1101 w	ν(CC) skeletal, trans conformation
1080 vw	1085 w	1078 w	1082 vw		1082 vw	ν(CC) skeletal, random conformation
1060 vw	1060 vw	1062 w				ν(CC) skeletal, trans conformation
1045 vw	1045 vw	1045 vw	1043 vw	1050 wsh	1045 vw	ν(CC) skeletal, cis conformation
1031 w	1030 w	1029 vw	1030 w	1028 msh	1032 vw	ν(CC) skeletal, cis conformation
1002 s	1002 ms	1002 ms	1003 m	1003 m	1003 w	ν(CC) aromatic
956 w	954 mssh	956 w	958 w	958 w	955 vw	ρ(CH$_3$); δ(CC) α-helix
935 w	937 m	935 w	933 w	935 w	935 w	ρ(CH$_3$) terminal; ν(CC) α-helix
900 vw	898 w	900 vw	900 vw		897 vw	ρ(CH$_2$)
				877 vw		ρ(CH$_2$)
852 w	851 m	851 w	850 mw	852 s	852 w	δ(CCH) aromatic
827 w	825 w	829 w	827 mw	829 m	827 w	δ(CCH) aliphatic
757 vw	759 vw	758 vw	757 w	758 mw	755 vvw	ρ(CH$_2$) in-phase
642 m	642 mw	643 m	641 m	641 m	643 vw	ν(CS)
619 w	621 mw	622 w	620 w	621 w	620 vw	ν(CS)
601 vwsh	605 vvw	600 vw		605 vw		ρ(CH) wagging
564 vw		561 wsh				ρ(CH) wagging
549 vw	549 vw			545 vvw		ν(S–S) trans–gauche–trans
541 vw	540 vw	539 vw				ν(S–S) trans–gauche–trans
	525 vvw			525 vvw		ν(S–S) gauche–gauche–trans
510 wbr	509 wbr	509 m	509 wbr	509 w	511 wbr	ν(S–S) gauche–gauche–gauche
490 w	490 w	490 w	489 w	492 w	491 w	ν(S–S) gauche–gauche–gauche

[a] s, strong; m, medium; w, weak; v, very; br, broad; sh, shoulder.

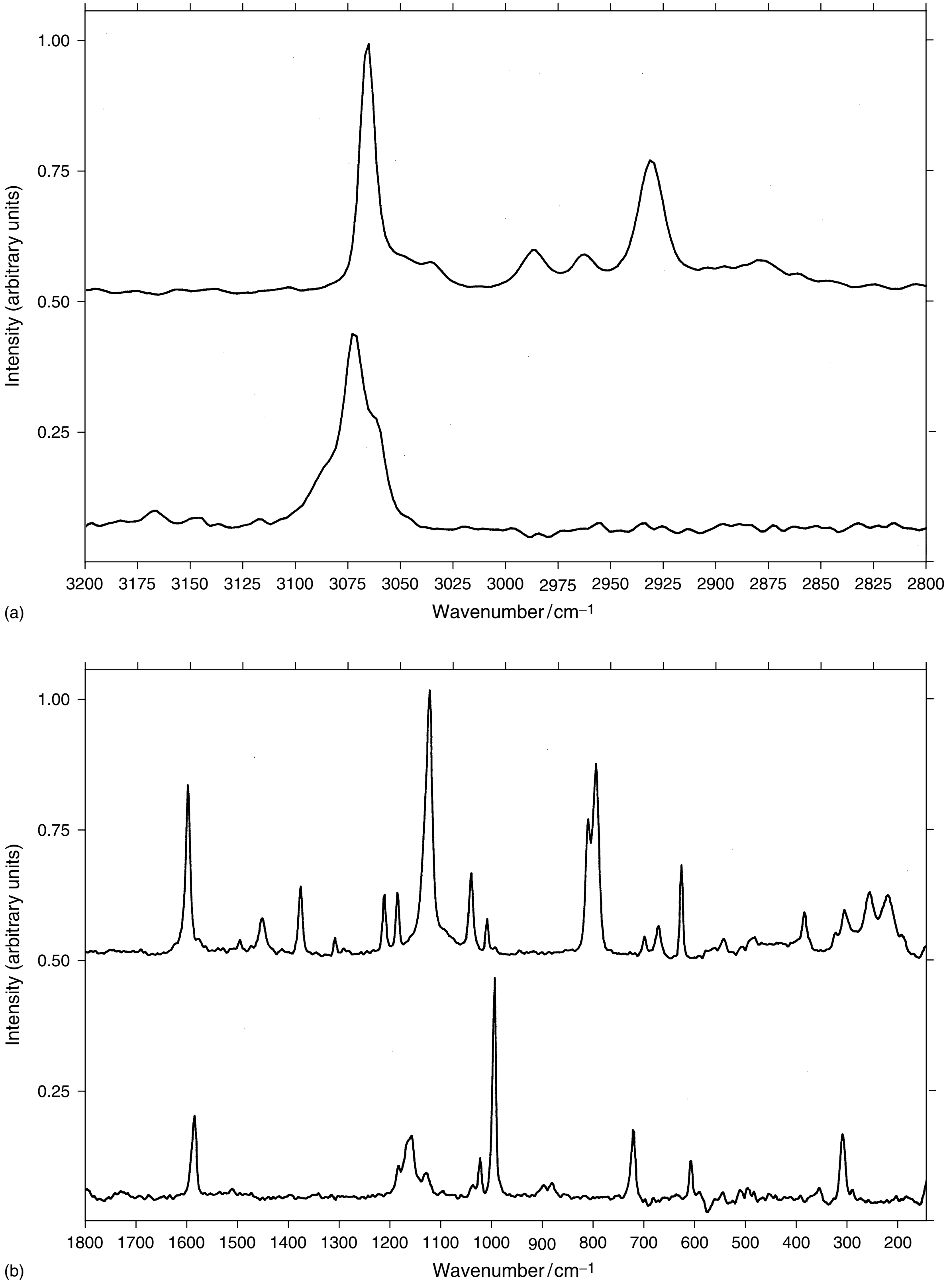

Figure 16. Fourier transform Raman spectra of *p*-toluenesulfonic acid (upper spectra) and benzenesulfonic acid (lower spectra), 1064 nm excitation: (a) wavenumber range 2800–3200 cm^{-1}; (b) wavenumber range 150–1800 cm^{-1}. Note the presence of the strong band at 3060 cm^{-1} in each spectrum, assigned to aromatic ν(C–H) stretching and the disappearance of the ν(C–C) aromatic ring breathing mode at 1003 cm^{-1} in the upper spectrum.

This article was published in the *Handbook of Vibrational Spectroscopy* in 2006 by John Wiley & Sons, Ltd.
DOI: 10.1002/9780470027325.s4103

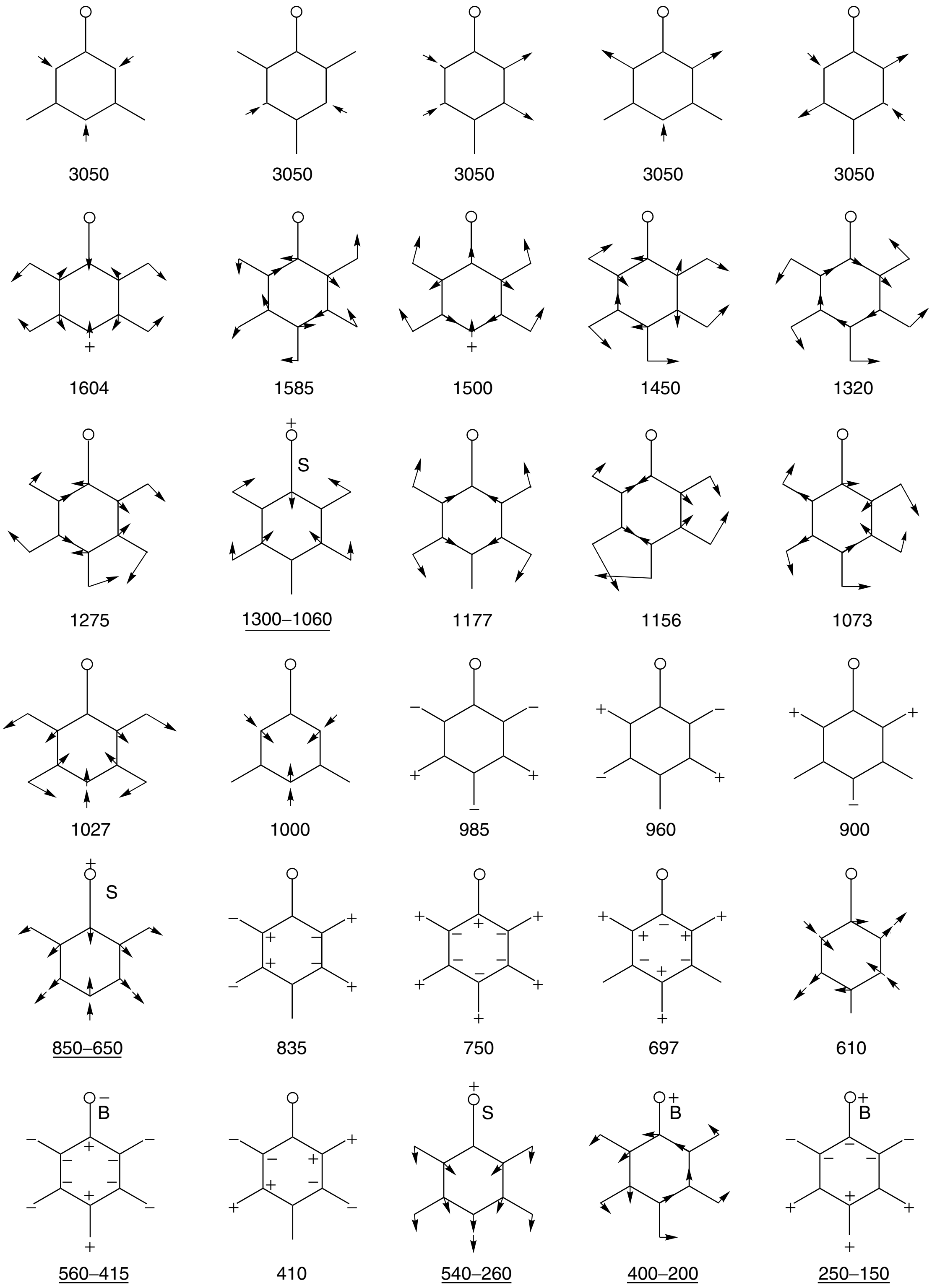

Figure 17. The 30 vibrational modes of benzene, only six of which (underlined) are substituent-sensitive and therefore useful for structural information about ortho, meta or para functionality. [Reproduced with permission of Academic Press Inc. from D. Lin-Vien, N.B. Colthup, N.G. Fateley and J.G. Grasselli, “Infrared and Raman Characteristics of Organic Molecules”, Academic Press Inc., San Diego, USA (1991).]

Aromatic ν(C–H) stretching bands, with some complexity and multiplicity in IR absorption, give rise to a single Raman band in the region 3030–3070 cm^{-1}. Often this is observed as a high-wavenumber feature on the broader aliphatic ν(C–H) multiplet centered near 2950 cm^{-1}, as seen in the *p*-TsOH spectrum in Figure 16. Figure 17 shows that no fewer than five identifiable discrete vibrational modes have Raman bands predicted near 3050 cm^{-1}.

As the spectral bands in the 1700–1000 cm^{-1} region indicate, δ(CCH) in-plane ring bending and ν(C–C) ring stretching modes give rise to a more complex picture. In the 1000–700 cm^{-1} region, the out-of-plane ring vibrations occur. The most important Raman-active substituent-insensitive bands for aromatic benzenoid compounds are given in Table 5.

Next to the aromatic ν(C–H) vibrations the next characteristic Raman bands for an aromatic compound occur as a doublet of medium-strong intensity in the 1550–1630 cm^{-1} region. These are termed quadrant-stretching vibrations – the most critical parameter for IR or Raman activity of these modes is the overall molecular symmetry, hence, for symmetrically substituted benzenes, as in benzene itself, such as the *p*-(1,4 disubstitution) and tetrasubstituted or hexasubstituted benzenoid compounds, there is a center of symmetry preserved and the quadrant stretching modes are Raman-active only, giving rise to a characteristic doublet near 1600 and 1580 cm^{-1}. In contrast, other quadrant modes are antisymmetric with respect to the center of symmetry and these are only allowed in IR absorption. In the special case of the symmetrically trisubstituted 1,3,5-benzenoid compounds, the three-fold symmetry axis results in the quadrant modes being doubly degenerate and giving rise to a single feature near 1600 cm^{-1}.

Table 5. Raman-active substituent-insensitive bands for benzenoid compounds. [Reproduced with permission of Academic Press Inc. from D. Lin-Vien, N.B. Colthup, W.G. Fateley and J.G. Grasselli, "Infrared and Raman Characteristic Frequencies of Organic Molecules", Academic Press Inc., San Diego, USA (1991).]

Benzenoid substitution	Wavenumber range / cm^{-1}	Raman band intensity
Mono, di and tri	1620–1585	m
Mono, di and tri	1590–1565	m
Mono – ortho and meta	1510–1470	w
Mono – para	1525–1480	w
Mono – ortho and meta	1465–1430	w
Mono – para	1420–1400	w
Mono – ortho, meta and para	1040–1020	s/m
Mono – meta; sym trisubstituted	1010–990	vs
Mono – para	650–630	m
Mono – ortho, meta and para	630–605	m

The so-called semicircle stretching vibrations are antisymmetric with respect to the center of molecular symmetry in substituted benzene compounds and the resulting doublet near 1500 and 1400 cm^{-1} is weak in Raman scattering.

The complex ring-stretching mode near 1000 cm^{-1} is often the strongest vibration in the Raman spectrum of a benzenoid compound; care must be adopted in using this band as a characteristic feature of aromatic compounds generally, as it is actually derived from a mixture of the 992 cm^{-1} symmetric ν(C–C) stretching and 1011 cm^{-1} antisymmetric ν(C–C) stretching modes in benzene itself. Table 6 gives an analysis of this Raman-active feature, which can be used to deduce useful structural information from Raman spectra of benzenoid compounds. A very significant observation from this table is the absence of the symmetric ν(C–C) mode near 1000 cm^{-1} for ortho- and paradisubstituted benzenes, which is strong in the Raman spectra of monosubstituted and metadisubstituted benzenes. The orthodisubstituted compounds have a strong band at 1055–1020 cm^{-1} whereas the para compounds have only a medium-intensity feature near 1160 cm^{-1}. Care should be taken with the interpretation of bands in this region of the Raman spectra as many important functional groups have significant Raman features here; good examples are ν(C–O) near 1060 cm^{-1}, ν(S–O) near 1050 cm^{-1} and ν(C–C) of long-chain aliphatic alkane groups and fatty acids near 1050 cm^{-1}.

Table 6. Characteristic ν(C–C) Raman-active bands for aromatic compounds in the 990–1200 cm^{-1} region. [Reproduced with permission of Academic Press Inc. from D. Lin-Vien, N.B. Colthup, W.G. Fateley and J.G. Grasselli, "Infrared and Raman Characteristic Frequencies of Organic Molecules", Academic Press Inc., San Diego, USA (1991).]

Monosubstituted benzenes (cm^{-1})	Raman activity	Ortho (cm^{-1})	Raman activity	Meta (cm^{-1})	Raman activity	Para (cm^{-1})	Raman activity
1010–990	vs			1010–990	vs	1180–1150	m
1040–1015	m	1055–1020	s	1100–1060	w		
1080–1065	w	1150–1100	w	1140–1065	w		
1170–1150	w	1170–1150	w	1180–1145	w		
1180–1170	w						

This article was published in the *Handbook of Vibrational Spectroscopy* in 2006 by John Wiley & Sons, Ltd.
DOI: 10.1002/9780470027325.s4103

Table 7. Substituent-sensitive Raman-active bands in monosubstituted benzenes. [Reproduced with permission of Academic Press Inc. from D. Lin-Vien, N.B. Colthup, W.G. Fateley and J.G. Grasselli, "Infrared and Raman Characteristic Frequencies of Organic Molecules", Academic Press Inc., San Diego, USA (1991).]

Substituent	1300–1060 cm^{-1}	850–650 cm^{-1}	560–415 cm^{-1}	540–260 cm^{-1}	400–200 cm^{-1}	250–150 cm^{-1}
NH_2	1277	818	504	531	385	233
OH	1230	812	507	532	–	240
F	1218	807	496	519	368	241
CH_3	1208	786	464	521	344	216
Cl	1083	702	467	418	297	196
SH	1097	698	461	413	280	188
Br	1071	673	460	315	254	181
I	1060	654	450	266	220	166

Unlike the IR spectra of substituted benzenoid compounds, the Raman spectra are quite simple below 900 cm^{-1}, because the phenyl group δ(C–H) wagging modes are absent. Quadrant in-phase bending vibrations of medium intensity, however, are Raman-active near 600 cm^{-1} for monosubstituted and paradisubstituted benzenes.

Of lesser importance in a general survey are the substituent-sensitive bands, but good comprehensive spectroscopic databases can be used to identify specific functionalities in benzenoid compounds. For example, some common substitutents are cited in Table 7, from which it is possible to identify functionalities from good-quality Raman spectra. All these bands are of medium-strong intensity in the Raman spectrum.

4 APPLICATIONS OF SPECTRA–STRUCTURE CORRELATIONS IN THE RAMAN SPECTRA OF REAL-WORLD SPECIMENS

In this section, the application of Raman spectral-structural correlations to real examples of some complexity are illustrated. In selection of the examples cited here, attention is directed to the information provided from the spectra, especially in the form of band wavenumbers and intensities and explanations of changes in these parameters.

4.1 Biodeterioration of rock substrata by invasive organisms

The ability of lichens, fungi and algae to create favorable microclimates for the successful colonization of natural and man-made rock and stone substrata is now recognized and vibrational Raman spectroscopy is playing a vital role in the assessment of the biodeteriorative strategies that are being adopted under often highly adverse conditions. Hence, the spectroscopic information that is provided from the Raman analysis of the complex lichen–substratal encrustations or mediaeval and Renaissance wall-paintings, or prehistoric rock art in American paleo-Indian cave shelters and on ecclesiastical structures, is assisting in the identification of the proper conservation procedures and strategies for the preservation of valuable art heritage.

The critical steps in the analysis of the spectra provide an excellent example of the spectroscopic procedures that are usually adopted for the examination of complex systems, and in this particular case involving the biological degradation of geological minerals, provides a good illustration of the viability of the Raman spectroscopic technique in providing information at low wavenumbers as well as the more normally accessed functionality region for organic moieties.

Figure 18 shows the Raman spectra at 1064 nm excitation of a *Dirina massiliensis* forma *sorediata* encrustation on a Renaissance fresco painted in 1560 in the Palazzo Farnese, Italy;[19] spectrum (a) is that of the upper surface of the encrustation and (b) is that of the lower surface. Approaching the lower spectrum in the usual way we can deduce the following information:

1. The broad ν(C–H) feature centered at 2935 cm^{-1} is aliphatic in origin.
2. The strongest band in the spectrum at 1523 cm^{-1}, and a weaker band at 1157 cm^{-1}, are assignable to the ν(C=C) and ν(C–C) vibrations of the conjugated unsaturated side chain of β-carotene.
3. The weaker sharp bands at 1480, 910 and 506 cm^{-1} are the ν(C=C), ν(C–C) and $\delta(CO_2)$ modes, respectively, of calcium oxalate monohydrate.

This article was published in the *Handbook of Vibrational Spectroscopy* in 2006 by John Wiley & Sons, Ltd.
DOI: 10.1002/9780470027325.s4103

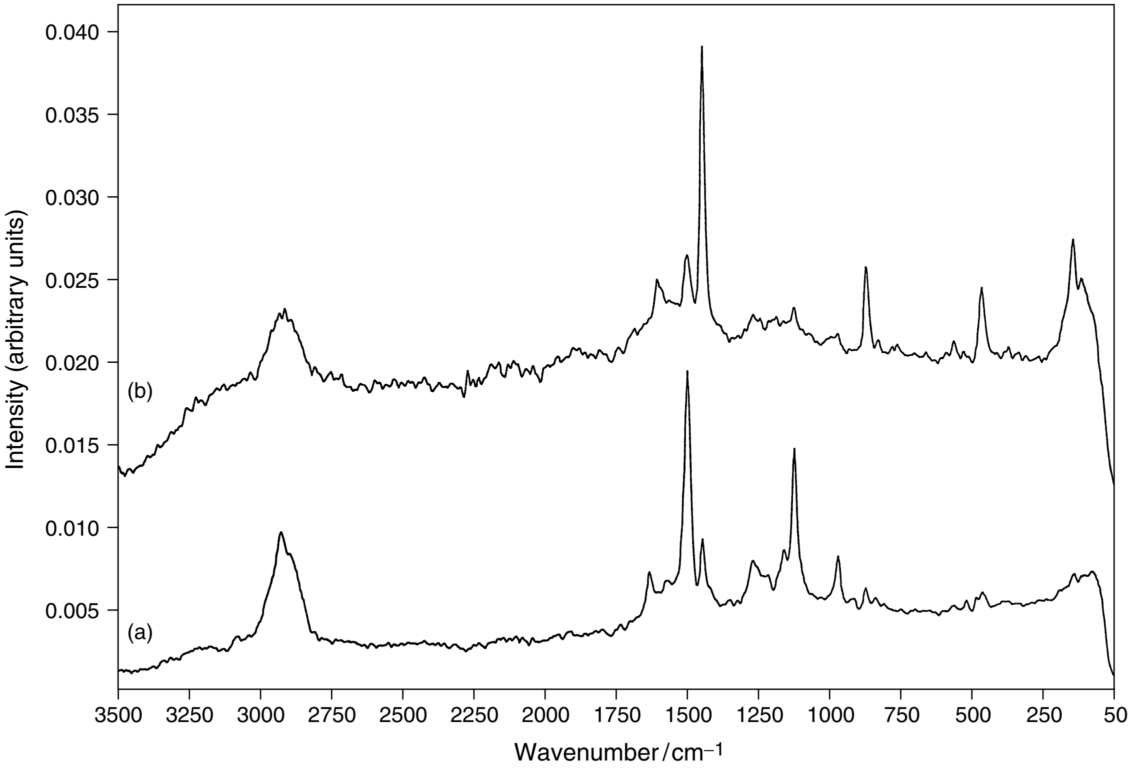

Figure 18. Fourier transform Raman spectra (1064 nm excitation) of *Dirina massiliensis* forma *sorediata* on Renaissance frescoes at the Palazzo Farnese, Caprarola, Italy: (a) upper surface, (b) lower surface. The effects of the production of oxalic acid by the lichen hyphae on the calcareous substrata can be clearly seen in (b), due to the appearance of the $\nu(\mathrm{C{=}O})$, $\nu(\mathrm{C{-}C})$ and $\delta(\mathrm{CO_2})$ modes of calcium oxalate monohydrate at 1480, 910 and 506 cm^{-1}, respectively.

4. Strong, sharp bands at 1086 and 1007 cm^{-1} arise from incorporated calcite and gypsum, respectively, and represent the $\mathrm{CO_3}^{2-}$ and $\mathrm{SO_4}^{2-}$ symmetric stretching modes.
5. A broad, weak feature centered near 760 cm^{-1} is ascribed to the calcium oxide/hydroxide used as a wall-preparation sealant for the fresco painting.[20]

The spectrum of the lower surface is rather different in that the strongest features now belong to the oxalate species in accord with the formation of calcium oxalate between oxalic acid from the mycobiont and the calcareous substratum.

This illustration demonstrates how the assignment of all major and minor vibrational bands in the Raman spectra can be undertaken; the recognition of these materials in the specimen provides the analyst with a dataset that can be used to compare with specimens from other sites and under other conditions. In such a way, a picture can be built up of chemical production in biodeterioration processes that can be assimilated by environmental scientists and conservators in their efforts to control the degradation and destruction of artwork and monuments (Figure 19).[19]

Figure 19. Lichen biodeterioration of the 16th century Renaissance frescoes at the Palazzo Farnese; in parts, some 80% of the artwork has been covered by *Dirina massiliensis* forma *sorediata*, which is capable of growing on pigments such as mercury(II) sulfide and arsenic(III) sulfide.

As different organisms produce different chemicals in their metabolic processes, the spectroscopic analytical approach is also useful in obtaining information about lichens growing under environmentally stressed conditions, such as the dry cold deserts of Antarctica. Figure 20 shows

DOI: 10.1002/9780470027325.s4103

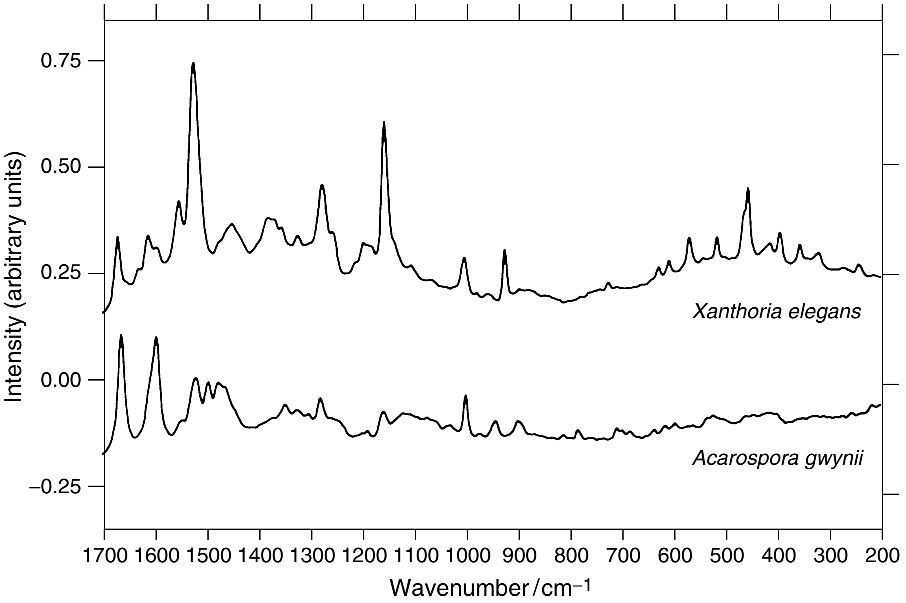

Figure 20. Raman spectra of two colored, epilithic lichens from Antarctica, *Xanthoria elegans* and *Acarospora gwynnii*, for the wavenumber range 200–1700 cm^{-1}.

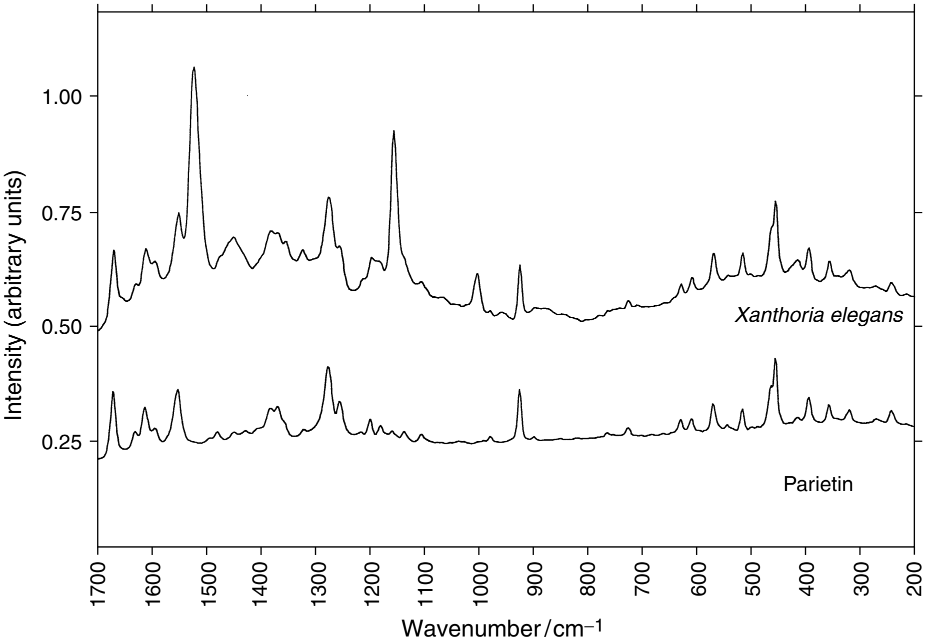

Figure 21. Fourier transform Raman stack-plot of the lichen *Xanthoria* and an important UV-protective pigment, paretin, which the organism produces to contrast UV radiation reaching the Antarctic surface through atmospheric ozone depletion. The major bands of parietin are clearly seen in the Raman spectrum of the living organism.

an FT-Raman stack-plot of two Antarctic epilithic lichen encrustations on East Beacon sandstone from the McMurdo Dry Valleys, Victoria Land, Antarctica; this illustrates the capability of the Raman spectroscopic method to identify the species of the biodeteriorating organism from the spectra of the chemical species produced. The upper spectrum is of a *Xanthoria elegans* growth and the lower one of *Acarospora gwynni*. Figure 21 illustrates a starting point in the procedure for the identification of the chemical components in these complex encrustations by comparison of the lichen encrustation with a key pigment, parietin; several bands characteristic of parietin are observed in the spectrum of the encrustation.[22]

This is a starting point for the investigation into the strategies used by organisms to combat environmental stresses such as UV radiation flux, temperature extremes, humidity

This article was published in the *Handbook of Vibrational Spectroscopy* in 2006 by John Wiley & Sons, Ltd.
DOI: 10.1002/9780470027325.s4103

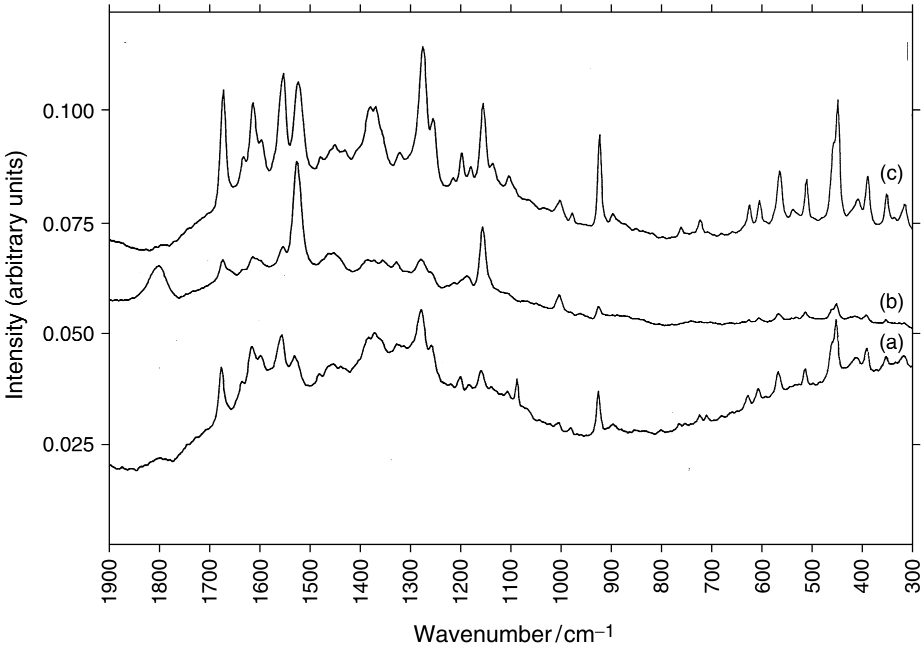

Figure 22. Fourier transform Raman structure–spectral correlations used in a geographical context. Spectra of *Xanthoria elegans* from three different Antarctic locations, showing the compositions of encrustation components, which reflect the different survival strategies operating from a Polar plateau to maritime to Antarctic ozone hole locations. [Reproduced with permission of Elsevier Science from Edwards, Holder and Wynn-Williams, *Soil Biol. Biochem.*, **30**, 1947–1953 (1998).]

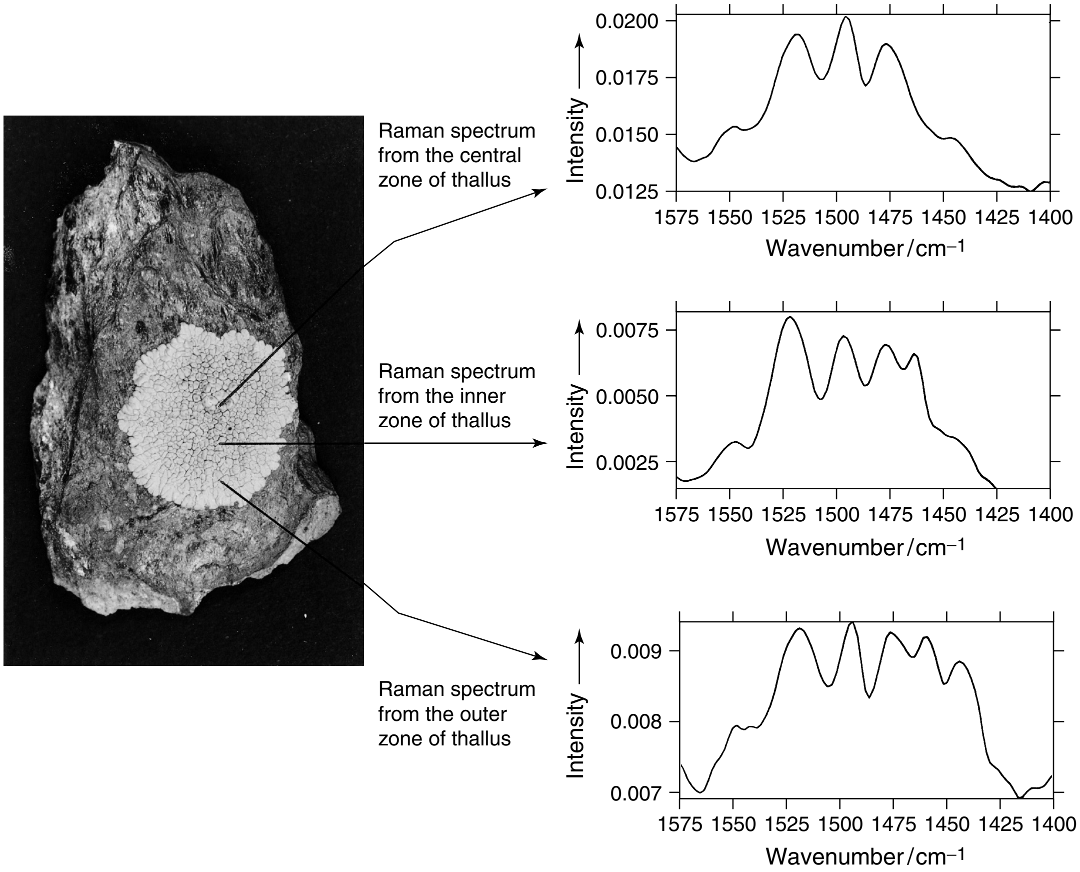

Figure 23. *Acarospora oxytoma* from the Sierra Nevada, Spain, elevation 2550 m. The three Raman spectra of the 1400–1575 cm^{-1} region illustrate the calcium oxalate mono- and dihydrate compositional variation and β-carotene pigmentation over the specimen surface.

This article was published in the *Handbook of Vibrational Spectroscopy* in 2006 by John Wiley & Sons, Ltd.
DOI: 10.1002/9780470027325.s4103

changes, and extreme desiccation. Figure 22 shows a stackplot of three *Xanthoria* Raman spectra from different Antarctic locations,[23] which involve extreme surface exposure to radiation under the atmospheric ozone hole, an edge situation to a sheltered Polar plateau environment. Figure 22(c) is from a maritime temperate location (outside the Antarctic zone), and the quality and detail should be noted. In contrast, Figures 22(a) and (b) are both from *Xanthoria* lichens from Antarctic locations under the ozone hole, from Harrow Peaks, Victoria Land, at 74 °S and 16 °E. The difference in these reflects the different aspect changes in the stressed environment. Figures 22(a) and (b) are very different from (c); this illustrates the effect of Antarctic locations on the ability of lichens to produce pigments and chemicals necessary for survival under different climatic conditions. The production of pigments, cryoprotectants and chemicals to combat desiccation can be identified in these spectra, including paretin and trehalose. Comparison can also be made in the spectra of lichens from hot deserts and cold deserts to evaluate the mechanisms adopted for survival in very different stress situations. Figure 23 shows an *Acarospora oxytoma* growth on sandstone from the Sierra Nevada, Spain and the Raman microscope spectra obtained from difficult thallial zones. Key features here are the $1523\,\mathrm{cm}^{-1}$ mode of β-carotene involving $\nu(\mathrm{C{=}C})$ stretching and the bands between 1460 and $1490\,\mathrm{cm}^{-1}$ characteristic of calcium oxalate monohydrate and dihydrate, $CaC_2O_4{\cdot}H_2O$ and $CaC_2O_4{\cdot}2H_2O$.[24] Clearly, there are different amounts of pigment and hydrated oxalate present in each of the three thallial zones sampled by the spectrometer, which reflects the balance made by the living organism between exposure to radiation and desiccation. From this has come the suggestion that hydrated calcium oxalate is used as a water storage device in periods of drought. Despite the fact that calcium oxalate monohydrate and dihydrate might have been expected to have had similar Raman spectra with only a small difference reflecting the water content, the reality (Figure 24) is very different. From this it is seen that the Raman spectra of $CaC_2O_4{\cdot}H_2O$ and $CaC_2O_4{\cdot}2H_2O$ are of very different appearance, especially in the $1400–1500\,\mathrm{cm}^{-1}$ region, which proves critical for the experiments on *Acaraspora* outlined above.[25]

The ability of some organisms to assist each other in surviving inhospitable environments (symbiosis) is also well illustrated by the Raman microscopic spectra of *Ochrolechia parella* and *Xanthioria parietina* in Figure 25. Here, the *Ochrolechia* spectrum indicates that a major production of calcium oxalate monohydrate is taking place, with the doublet feature near $1500\,\mathrm{cm}^{-1}$. In contrast, the *Xanthoria* lichen produces little calcium oxalate, but a major effort has gone into the produce of the radiation protectant parietin.[26] Hence, Raman spectroscopy provides some novel information about how species can co-exist in a supportive symbiotic role when either one individually

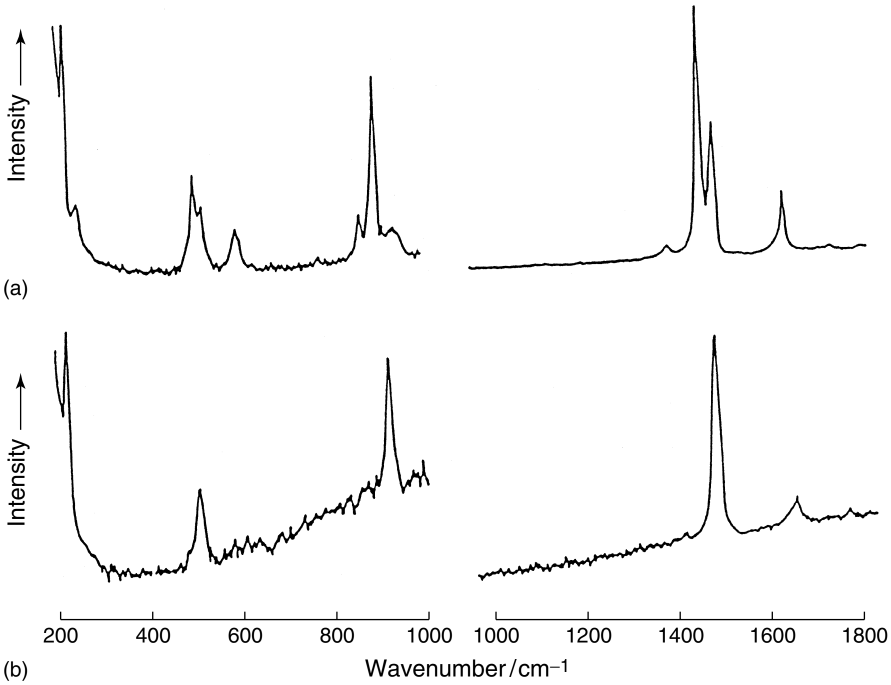

Figure 24. Raman spectra of (a) $CaC_2O_4{\cdot}H_2O$ and (b) $CaC_2O_4{\cdot}2H_2O$ showing the capability of structure-spectral correlation in the differentiation of the state of hydration of a geological material, despite the Raman spectrum of water itself being weak. [Reproduced with permission of J. Wiley & Sons Ltd., from H.G.M. Edwards, D.W. Farwell, R. Jenkins and M.R.D. Seaward, *J. Raman Spectroscopy*, **23**, 185–189 (1992).]

DOI: 10.1002/9780470027325.s4103

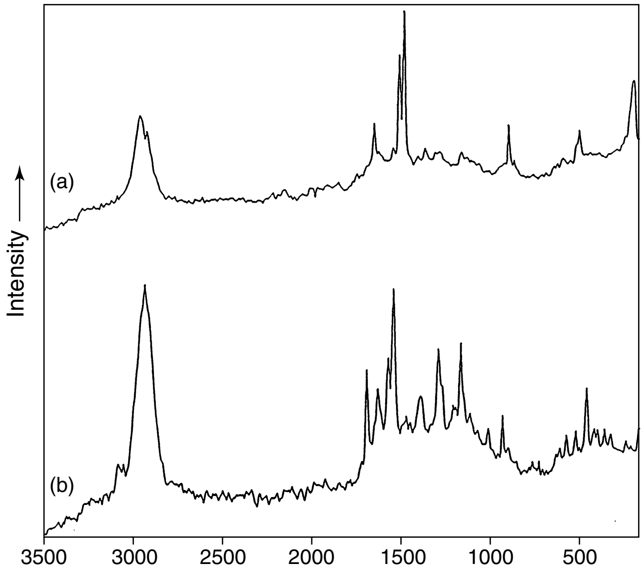

Figure 25. Fourier transform Raman spectra of (a) *Ochrolechia parella* and (b) *Xanthoria parietina* on sandstone; 1064 nm excitation, 200–3500 cm^{-1} excitation. The symbiosis of these two organisms is understood from the analysis of the Raman spectra as *Ochrolechia* provides a means of substratal biodeterioration and colonization via calcium oxalate production, while the *Xanthoria* provides the photoprotective pigment production of the colony. [Reproduced with permission of J. Wiley & Sons, from H.G.M. Edwards, K.A.E. Edwards, D.W. Farwell, I.R. Lewis and M.R.D. Seaward, *J. Raman Spectroscopy*, **25**, 99–103 (1994).]

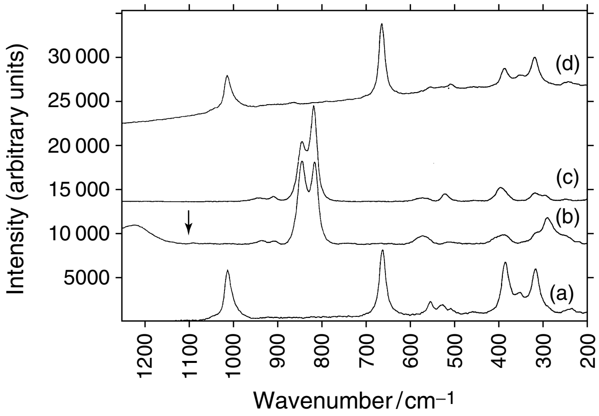

Figure 26. Raman microscope spectra of Nakhla meteorite specimens. (a) Black particle, (b) white particle, (c) brown, glassy particle, (d) clear, glassy particle. The heterogeneity of the specimen should be noted; bands at 320, 350, 386, 662 and 1009 cm^{-1} are characteristic of clinopyroxene, 815 and 841 cm^{-1} of olivine, and 508 and 520 cm^{-1} of plagioclase. The very weak band at 1086 cm^{-1} in spectrum (b) is significant as it indicates the presence of a carbonate. [Reproduced with permission of Elsevier Science from H.G.M. Edwards, D.W. Farwell, M.M. Grady, D.D. Wynn-Williams and I.P. Wright, *Planetary Space Sciences*, **47**, 353–362 (1999).]

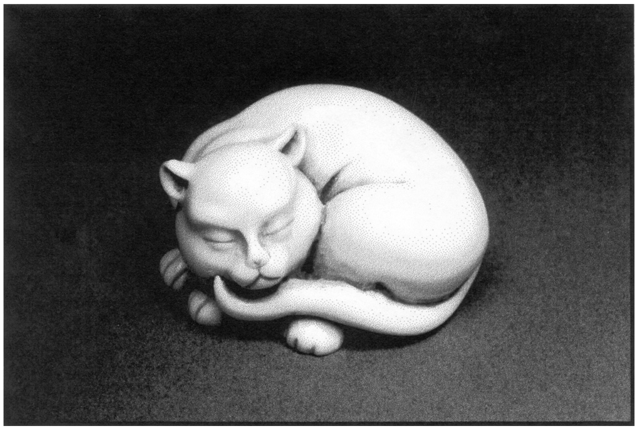

Figure 27. A cat, supposedly made of elephant ivory, found associated with some ancient artefacts and subjected to nondestructive Raman spectroscopic analysis. [Reproduced with permission of Elsevier Science from H.G.M. Edwards and D.W. Farwell, *Spectrochimica Acta, Part A*, **51**, 2073–2082 (1995).]

would be at risk from environmental stresses. The production of calcium oxalate monohydrate by an endolithic species, which has colonized chasms and fissures inside sandstone rocks to escape harsh surface temperatures and radiation, has been illustrated in an East Beacon Antarctic cryptoendolith.

4.2 Martian meteorites

The importance of the establishment of a Raman spectral database for the foundation of spectral-structure correlations is paramount. It is quite clear, also, that there is no single text currently available that will cover all possible eventualities from minerals, inorganic, organic and organometallic coordination compounds, solutions, polymers and biomaterials. Hence, an integral part of most projects still involves the acquisition of Raman data from standards and model compounds from which the deductions about structure can be informed.

A topical example of this process is provided by the planned exploration of Mars (and possibly Europa) using unmanned, robotic vehicles and landers that will contain specially selected suites of instrumentation for analytical studies. The challenge facing the analysts is great; for the first time, Raman spectrometers have been proposed successfully as part of an en suite space mission and the criteria for their constitution, ruggedness, operational regimes and information retrieval capabilities are some of the most demanding ever proposed for spectroscopists.[27,28] These experiments in remote Raman spectroscopy will compromise the most challenging yet undertaken for Raman work – with Martian surface radiation levels, temperature fluctuations, dust clouds and wind storms posing severe problems for operational viability. Because of the highly

DOI: 10.1002/9780470027325.s4103

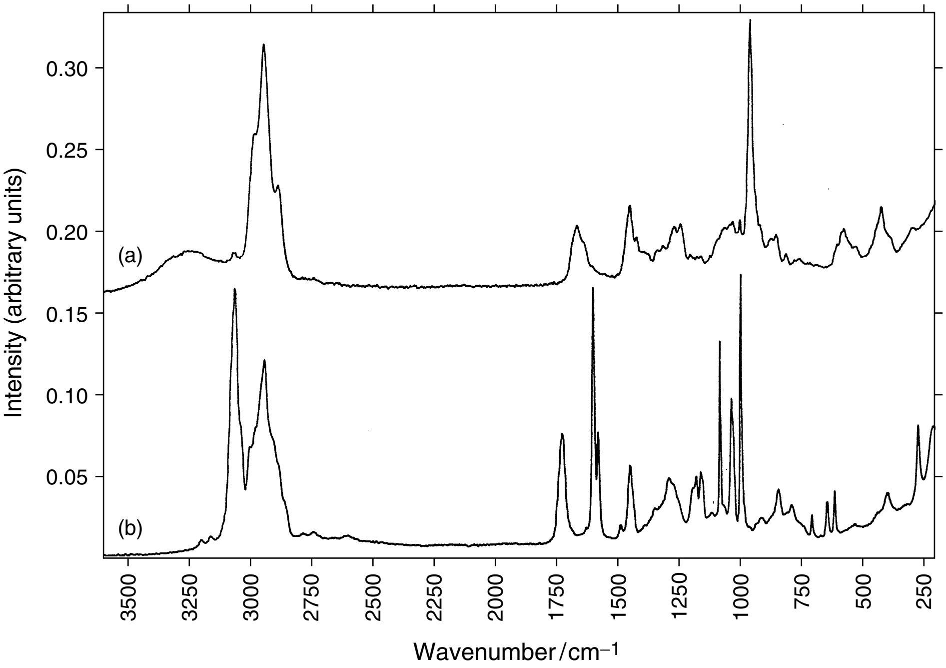

Figure 28. Fourier transform Raman spectra of (a) genuine elephant ivory and (b) the cat carving shown in Figure 27. Clearly, the cat is a clever forgery; bands at 3060, 1725, 1590 and 1003 cm^{-1} identify the specimen as a polymer resin consisting of polymethylmethacrylate and polystyrene. An additional band at 1086 cm^{-1} indicates that powdered calcite has been added to the resin to simulate the texture and density of genuine ivory.

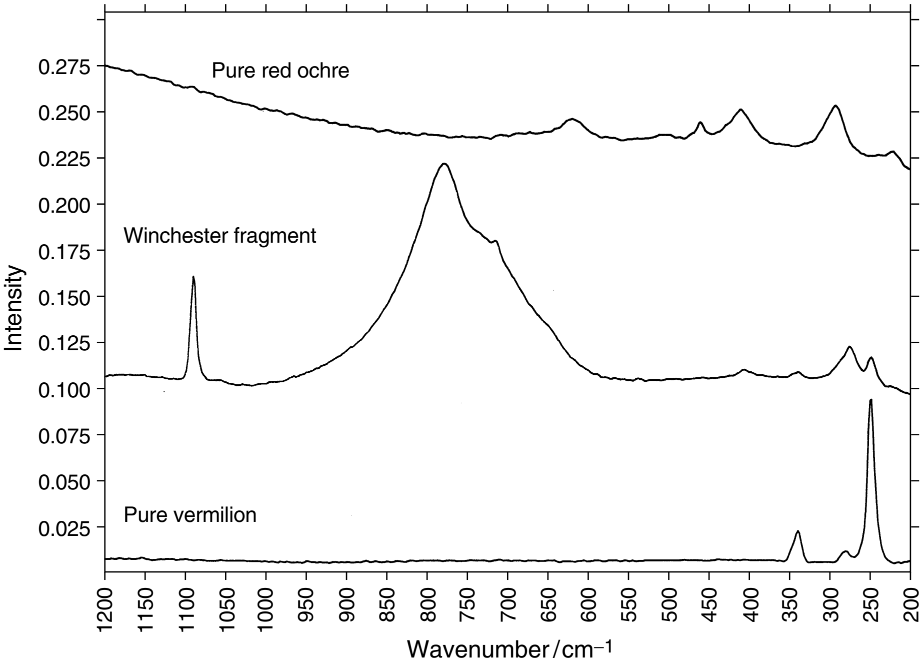

Figure 29. Fourier transform Raman spectra of red ochre (an iron(II) oxide–clay and sand mixture) pure vermilion (mercury(II) sulfide) and a red pigment fragment from the early mediaeval wall paintings in Winchester Cathedral, UK. The adulteration of the expensive cinnabar with cheap hematite is observed in the ecclesiastical sample. The sharp bands at 1086 and 760 cm^{-1} in this spectrum arise from the procedures used in application of the pigment to the wall substratum – a limewash consisting of calcium oxide, calcium hydroxide and calcite dust was used as a fine coat prior to the painting being undertaken. [Reproduced with permission of J. Wiley & Sons Ltd., from H.G.M. Edwards, C. Brooke and J.K.F. Tait, *J. Raman Spectroscopy*, **28**, 95–98 (1997).]

DOI: 10.1002/9780470027325.s4103

reactive and oxidizing nature expected for the Martian regolith, it is expected that little is to be found there of biochemical interest; however, at distances beneath the Martian surface and in the shelter of large rocks the situation may apply that organic molecules may have survived in the so-called fossil record.

Several groups worldwide have addressed the problem of miniaturization of Raman spectrometers for robotic Martian exploration. The acquisition of Raman data relevant to this project in the form of databases is also proceeding apace. Here, we demonstrate how Raman spectral-structural correlations for Martian material and simulates will provide useful case studies on which the future interpretation of Martian Raman analyses will depend. For this work, it is fortunate that some 13 samples of actual extraterrestrial Martian geology now exist on Earth in the form of the Shergotty–Nakhla–Chassigny Martian meteorites. Of these, the Allen Hills and Nakhla meteorites are famous examples; these have been studied in our laboratories.[29]

Figure 26 shows a stack-plot Raman microscopic spectral comparison of different regions of a fragment of the Nakhla meteorite, which fell in Egypt in 1911. The heterogeneity of the specimen is clear; the presence of the silicates, plagioclase and olivine is recognized by the features near 800 cm^{-1} and quartz particles by the bands at 465 and 206 cm^{-1}.[29] It is frequently the case spectroscopically that the weakest bands contain important information and that is also manifest here; the very weak band at 1086 cm^{-1} (indicated by an arrow on curve b) is indicative of calcium carbonate in the meteorite. As this meteorite is confirmed as having originated from Mars, and was probably ejected from the Martian surface by impact of an asteroid or similar object, the observation of carbonate inside the meteorite fragment strongly suggests that at that period of Martian history (about 1.6 Bya) there was water on Mars, which may have supported primitive life forms. This is an important and controversial conclusion from the observation of a very weak Raman band and application of spectral-structural

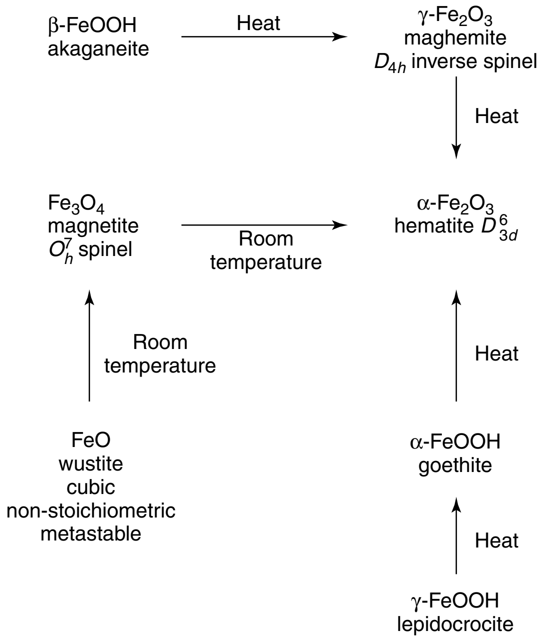

Figure 30. Minerals in the iron oxide/hydroxide system that were used as pigments in antiquity. [Reproduced with permission of Elsevier Science from H.G.M. Edwards, E.M. Newton and J. Russ, *J. Molecular Structure*, **550/551**, 245 (2000).]

Table 8. Raman band wavenumber ranges for important inorganic materials. [Tables (b) (c) and (d) reproduced with permission of Academic Press Inc. from K. Nakamoto, "Infrared and Raman Spectra of Inorganic and Coordination Compounds", Academic Press Inc., San Diego, USA (1997).]

(a) Modes involving hydrogen

Wavenumber range / cm^{-1}	Vibrational mode	Functionality
4000–3000	H–F stretching	Hydrogen fluorides
3750–3100	O–H stretching (symmetric and antisymmetric)	Hydroxyl groups
3550–3050	N–H stretching	Amino and imino compounds
3100–2800	C–H stretching (symmetric and antisymmetric)	Metal methyls
3000–2500	H–Cl stretching	Hydrogen chlorides
2700–2500	S–H stretching	Thiols, sulfhydrides
2650–2400	H–Br stretching	Hydrogen bromides
	H–B stretching	Terminal boranes
2500–2200	P–H and Se–H stretching	Phosphines and hydrosglenides
2300–2100	H–I stretching	Hydrogen iodides and arsines
2250–2100	H–Si stretching	Silanes
2175–2050	H–Ge stretching	Germanes
1800–1700	H–Al stretching	Aluminum hydrides

(*continued overleaf*)

Handbook of Vibrational Spectroscopy, Online © 2006 John Wiley & Sons, Ltd.
This article is © 2006 John Wiley & Sons, Ltd.
This article was published in the *Handbook of Vibrational Spectroscopy* in 2006 by John Wiley & Sons, Ltd.
DOI: 10.1002/9780470027325.s4103

Table 8. (*Continued*)

(b) Oxygen stretching and bending frequencies.

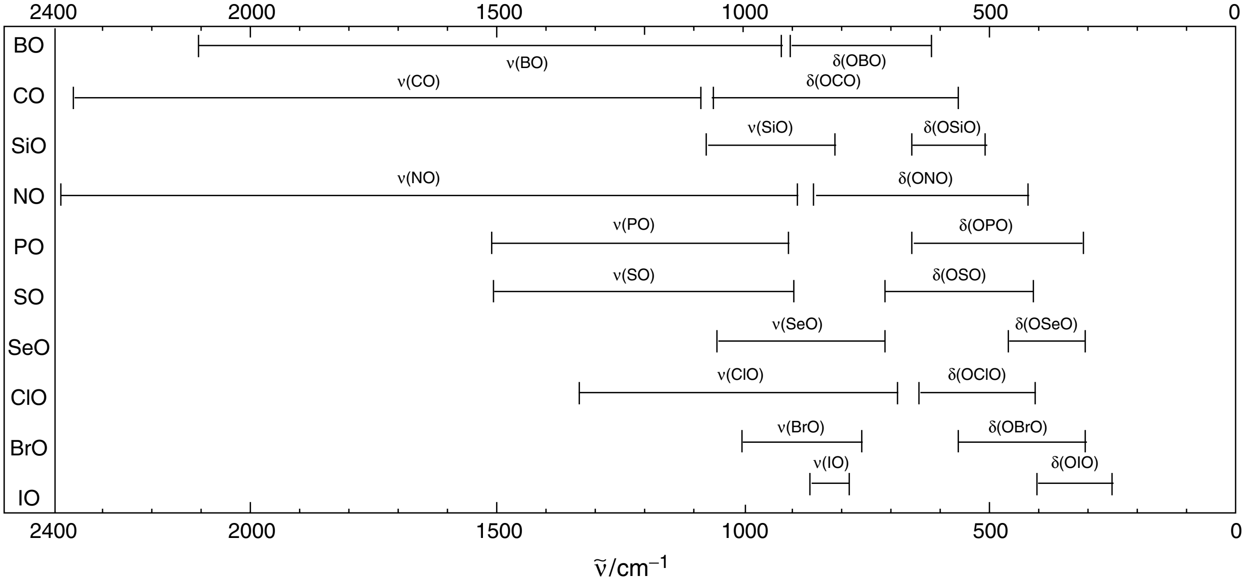

(c) Halogen (X) stretching frequencies.

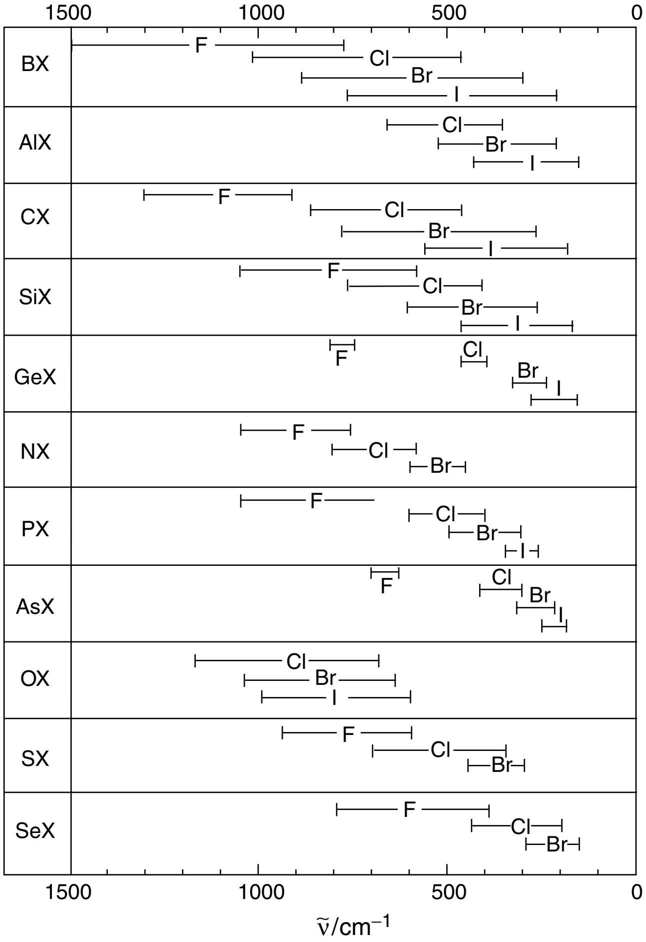

Handbook of Vibrational Spectroscopy, Online © 2006 John Wiley & Sons, Ltd.
This article is © 2006 John Wiley & Sons, Ltd.
This article was published in the *Handbook of Vibrational Spectroscopy* in 2006 by John Wiley & Sons, Ltd.
DOI: 10.1002/9780470027325.s4103

Table 8. (*Continued*)

(d) Characteristic frequencies of some inorganic ions. (Broken lines indicate Raman active vibrations.)

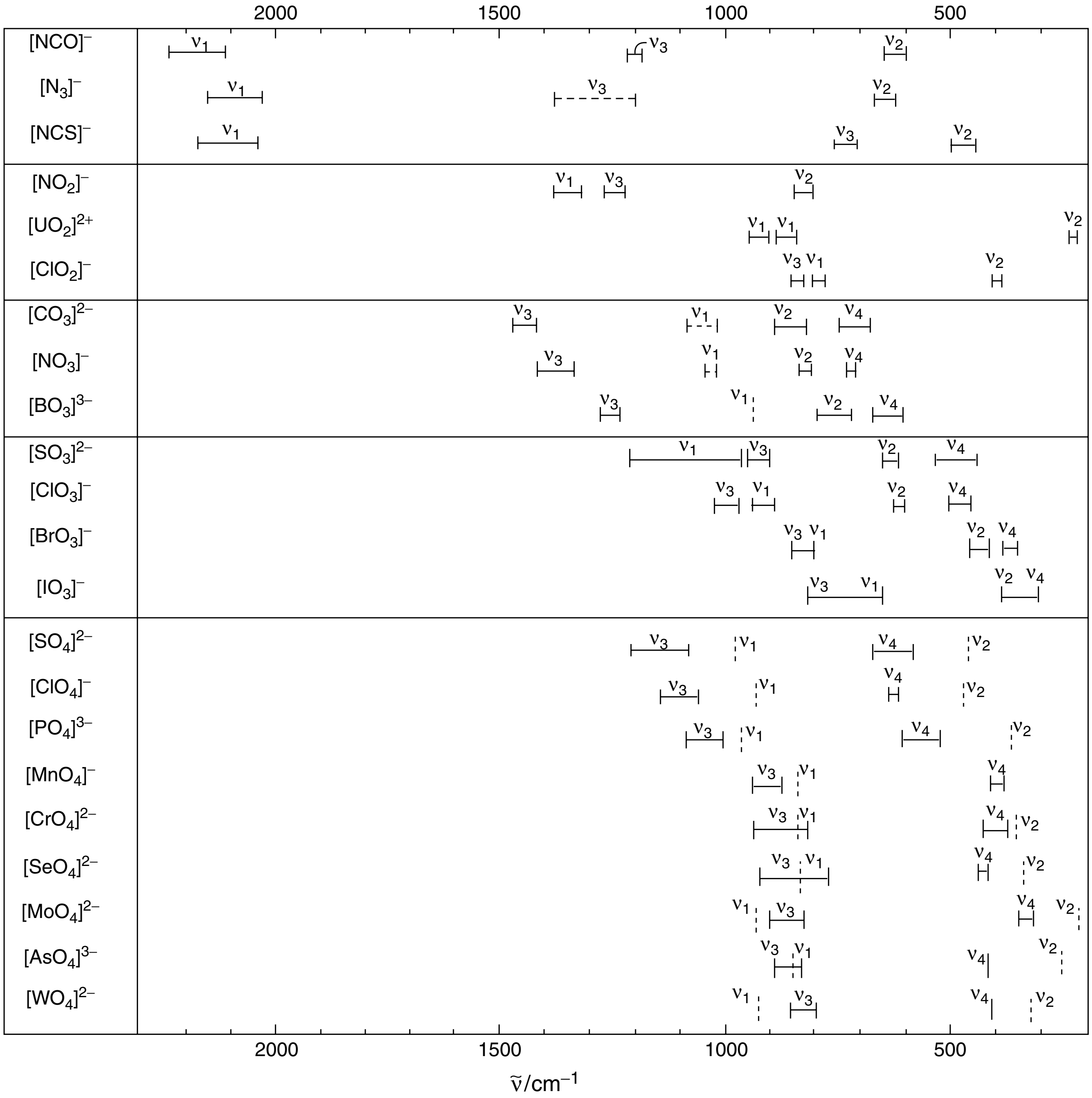

correlations! The presence of carbonate has recently been confirmed in the Nakhla meteorite using other analytical techniques.

4.3 Spectral-structural correlations for the identification of genuine works of art

An illustration of the practical application of Raman spectral-structural correlations for the identification of genuine or fake works of art is provided by recent studies of ivory. Earlier in this article, the Raman spectrum of ivory was cited as a biomaterial in which collagen was interspersed within a hydroxyapatite matrix (primarily calcium phosphate). The worldwide ban on importation of ivory designed to protect threatened animal species has been successful, but has generated attempts to fake ivory for material gain. A classic example is provided by the reclining cat figure in Figure 27, which was believed to be a valuable historical piece, having been found associated with other apparently genuine artefacts. The Raman spectrum of the cat[30] is shown alongside that of genuine elephant ivory in Figure 28; clearly, the two spectra are very different. The cat is not ivory and the Raman spectra indicate that it is a resin compound of polymethylmethacrylate with polystyrene; the unique feature about this spectrum, however, are the bands at 1086, 712 and 280 cm^{-1}, which are characteristic of calcium carbonate. It is apparent that the faker has mixed calcite with the resin to simulate the color, texture and density of genuine ivory; as the resin components are twentieth century materials, the cat cannot be considered as a genuine eighteenth century artefact any longer.

The use of spectral-structural correlations for wall-paintings and historiated manuscripts has been mentioned. In the example shown in Figure 29, the Raman spectrum of a specimen of red pigment from a mediaeval English wall-painting from Winchester Cathedral is shown;[31] this dates from about 1175 AD and is interesting because it clearly shows evidence of heavy adulteration of the very expensive cinnabar (vermillion) pigment by cheap iron ochre (hematite). The various forms of iron(III) oxide/hydroxide[32] used for pigments are shown in Figure 30. It is estimated from calibration experiments that the cinnabar has been mixed with hematite in the ratio 1 : 9! In similar studies of paint fragments from Spanish wall paintings and frescoes, we have found evidence of retouching of paint work, which must have occurred in later times; the reason for this, it transpires, has been an attempt to restore fading or deteriorating artwork which has been subjected to environmental degradation as a result of its proximity to unglazed windows.

5 WAVENUMBER AND FUNCTIONALITY CORRELATIONS

Band wavenumber ranges for some common chemical bonds for organic and inorganic compounds are collected in Tables 2 and 8, respectively. These tables are a common feature of many texts for practical vibrational spectroscopy and undoubtedly have a prime purpose in structure identification; however, care must be exercised in their use because unambiguous band assignment is rarely possible unless supporting information is also forthcoming. This can be provided from other spectroscopic or diffraction techniques and scanning electron microscopy (SEM) or energy dispersive low-angle X-ray scattering (EDAXS) data are also extremely useful for confirming the presence or otherwise of certain elements. Hence, for example, it is ineffectual to suggest the presence in an ancient pigment of lead white, basic lead carbonate $Pb(OH)_2 \cdot PbCO_3$, solely from the presence of a Raman band at 1050 cm^{-1} from a white powder. If the material does not contain lead or carbonate, this band could equally well be assignable to a ν(C–C) of an extended lipid chain, a ν(C–OH) mode of an alcoholic group or a $\nu(S–O_3{}^{-})$ symmetric stretching mode of an aromatic sulfonate, such as sodium benzene sulfonate.

The problem of confidence in band assignment is exacerbated for wavenumber shifts of less than 1000 cm^{-1} because here the inorganic/organic modes are truly open to confusion in complex systems. For example, is a band at 505 cm^{-1} a $\delta(CO_2)$ of a metal oxalate, a ν(S–S) of a keratotic biopolymer, a ν(Si–O) of an orthosilicate or a ν(M–C) metal–carbon stretching of an organometallic compound? This problem can also arise in organic chemistry where the identification of ν(M–P) and ν(M–Cl) of metal–phosphine and metal–chlorine coordination is well known, with bands in the 250–400 cm^{-1} region being assigned ambiguously. A solution to the problem is often afforded by recourse to the spectra of a database of model compounds that contain similar groupings to the material under investigation and, generally, this procedure combined with some form of elemental composition is sufficient to direct the analytical spectroscopist towards the exclusion of some otherwise feasible possibilities.

ABBREVIATIONS AND ACRONYMS

EDAXS	Energy Dispersive Low-angle X-ray Scattering
DMTD	2,5-Dimercapto-1,3,4-Thiadiazole
PBB	Polybutadienes
p-TsOH	4-Toluenesulfonic Acid
RRS	Resonance Raman Scattering
SEM	Scanning Electron Microscopy

REFERENCES

1. K. Asselin and D.B. Chase, *Appl. Spectrosc.*, **48**, 6 (1994).
2. H.G.M. Edwards, 'Art Studies: Application of Infrared and Raman Spectroscopy', in "Encyclopaedia of Spectroscopy and Spectrometry", eds J.C. Lindon, G.E. Tranter and J.L. Holmes, Academic Press, London, 649–657 (1999).
3. H.G.M. Edwards, 'Raman Spectroscopy: Instrumentation', in "Encyclopaedia of Applied Physics", ed. G. Trigg, Wiley/VCH Publishers, Weinheim and New York, 1–43, Vol. 16 (1996).
4. H.G.M. Edwards, A.C. Williams, D.W. Farwell, B.W. Barry and F. Rull, *J. Chem. Soc., Faraday Trans.*, **91**, 3883 (1995).
5. H.G.M. Edwards, 'Applications of Raman Spectroscopy to Archaeology', in "Proceedings of the XVIth International Conference on Raman Spectroscopy (ICORS XVI)", Cape Town, South Africa, ed. A.M. Heyns, J. Wiley & Sons, Chichester, 81–84 (1998).
6. S.P. Best, R.J.H. Clark and R. Withnall, *Endeavour*, (New Series), **16**, 66 (1992).
7. D.C. Smith, H.G.M. Edwards, M. Bouchard, R.H. Brody, F. Rull Perez, R. Withnall and C. Coupry, "MRM (Mobile

Handbook of Vibrational Spectroscopy, Online © 2006 John Wiley & Sons, Ltd.

This article was published in the *Handbook of Vibrational Spectroscopy* in 2006 by John Wiley & Sons, Ltd.
DOI: 10.1002/9780470027325.s4103

Raman Microscopy): A Powerful Nondestructive *In Situ* Archaeometric Tool for Microspectrometrical Analysis of Cultural Heritage (ARCHAEORAMAN): Geomaterials, Biomaterials and Pigments", Proceedings of the 2nd International Conference on Science and Technology for the Safeguard of Cultural Heritage, University of Paris X-Nanterre, in press (2000).

8. P.J. Hendra and J.K. Agbenyega, 'The Raman Spectra of Polymers', J. Wiley & Sons, Chichester (1993).
9. B. Schrader, 'Infrared and Raman Spectroscopy: Methods and Applications', VCH Publications, Weinheim and New York (1995).
10. S. Poshyachinda, H.G.M. Edwards and A.F. Johnson, *Polymer*, **32**, 334 (1991).
11. S. Poshyachinda, H.G.M. Edwards and A.F. Johnson, *Polymer*, **32**, 338 (1991).
12. M. Veronelli, G. Zerbi and R. Stradi, *J. Raman Spectrosc.*, **26**, 683 (1995).
13. N.C. Russell, H.G.M. Edwards and D.D. Wynn-Williams, *Antarctic Science*, **10**, 63 (1998).
14. E.E. Lawson, H.G.M. Edwards and A.F. Johnson, *J. Raman Spectrosc.*, **26**, 617 (1995).
15. W. Qian and S. Krimm, *J. Raman Spectrosc.*, **23**, 517 (1992).
16. H.G.M. Edwards, D.E. Hunt and M.G. Sibley, *Spectrochim. Acta, Part A*, **54**, 745 (1998).
17. M. Gniadecka, H.C. Wulf, N. Nymark Morteisen, O. Fauskov Nielsen and D.H. Christensen, *J. Raman Spectrosc.*, **28**, 125 (1997).
18. D. Lin-Vien, N.B. Colthup, W.G. Fateley and J.G. Grasselli, 'Infrared and Raman Characteristic Frequencies of Organic Molecules', Academic Press Inc., San Diego, USA (1991).
19. M.R.D. Seaward and H.G.M. Edwards, *Cryptogamic Botany*, **5**, 282 (1995).
20. H.G.M. Edwards, D.W. Farwell and S. Rozenberg, *J. Raman Spectrosc.*, **30**, 361 (1999).
21. D.D. Wynn-Williams, N.C. Russell and H.G.M. Edwards, 'Moisture and Habitat Structure as Regulators for Microalgal Colonists in Diverse Antarctic Terrestrial Habitats', in "Ecosystem Processes in Antarctic Ice-Free Landscapes", eds W.B. Lyons, C. Howard-Williams and J. Hawes, Balkema Press, Amsterdam, 77–88 (1997).
22. H.G.M. Edwards, J.M. Holder and D.D. Wynn-Williams, *Soil Biol. Biochem.*, **30**, 1947 (1998).
23. H.G.M. Edwards, J.M. Holder and D.D. Wynn-Williams, 'FT-Raman Spectroscopic Studies of Highly-coloured Lichen Species from the Antarctic', in "Proceedings of the XVIth Intl. Conference on Raman Spectroscopy (ICORS XVI)", Cape Town, South Africa, ed. A.M. Heyns, J. Wiley & Sons, Chichester, 534–535 (1998).
24. J.M. Holder, D.D. Wynn-Williams, F. Rull Perez and H.G.M. Edwards, *New Phytol.*, **145**, 271 (2000).
25. H.G.M. Edwards, N.C. Russell and M.R.D. Seaward, *Spectrochim. Acta, Part A*, **53**, 99 (1997).
26. H.G.M. Edwards, K.A.E. Edwards, D.W. Farwell, I.R. Lewis and M.R.D. Seaward, *J. Raman Spectrosc.*, **25**, 99–103 (1994).
27. D.D. Wynn-Williams, 'Antarctica as a Model for Ancient Mars', in "The Search for Life on Mars", ed. J.A. Hiscox, British Interplanetary Society, London, 49–57 (1999).
28. H.G.M. Edwards and E.M. Newton, 'Application of Raman Spectroscopy to Exobiological Prospecting', in "The Search for Life on Mars", ed. J.A. Hiscox, British Interplanetary Society, London, 83–88 (1999).
29. H.G.M. Edwards, D.W. Farwell, M.M. Grady, D.D. Wynn-Williams and I.P. Wright, *Planetary Space Sciences*, **47**, 353 (1999).
30. H.G.M. Edwards and D.W. Farwell, *Spectrochim. Acta, Part A*, **51**, 2073 (1995).
31. H.G.M. Edwards, C. Brooke and J.K.F. Tait, *J. Raman Spectrosc.*, **28**, 95 (1997).
32. H.G.M. Edwards, E.M. Newton and J. Russ, *J. Mol. Struct.*, **550/551**, 245 (2000).
33. K. Nakamoto, 'Infrared and Raman Spectra of Inorganic and Coordination Compounds', 5th edition, Wiley-Interscience, New York (1999).

Handbook of Vibrational Spectroscopy, Online © 2006 John Wiley & Sons, Ltd.

This article was published in the *Handbook of Vibrational Spectroscopy* in 2006 by John Wiley & Sons, Ltd.

DOI: 10.1002/9780470027325.s4103